

Lung Cancer: PET, Perfusion CT, and Functional MR Imaging

29

Santiago E. Rossi, Carmen Trinidad,
and Antonio Luna

Contents

29.1	Introduction	724
29.2	Diagnosis	724
29.3	Staging	726
29.3.1	Regional Lymph Nodes	727
29.3.2	Metastatic Disease	728
29.4	Prognosis and Therapeutic Response	730
29.5	Recurrent Lung Cancer	733
29.6	Functional MRI	733
29.6.1	Diffusion-Weighted MRI (DWI).....	733
29.6.2	Dynamic Contrast-Enhanced MRI (DCE-MRI)	737
29.7	Perfusion CT	741
29.7.1	Technique.....	741
29.7.2	Clinical Applications	741
	Conclusions	745
	References	745

Abbreviations

ADC	Apparent diffusion coefficient
AUC	Area under the curve
BF	Blood flow
BV	Blood volume
CT	Computed tomography
DCE-MRI	Dynamic contrast enhanced magnetic resonance imaging
DWI	Diffusion-weighted imaging
DWIBS	Diffusion-weighted imaging with background tissue suppression
FDG	Fluoro-deoxy-glucose
GE	Gradient-echo
GGOs	Ground glass opacities
HU	Hounsfield units
IVIM	Intravoxel incoherent motion
K^{ep}	Outflow rate constant
K^{trans}	Inflow transfer constant
MRI	Magnetic resonance imaging
MTT	Mean transit time
MVD	With micro-vessel density
NSCLC	Non-small cell lung cancer
PET	Positron emission tomography
PMB	Permeability
QT	Chemotherapy
RT	Radiotherapy
SCLC	Small cell lung cancer
SS EPI	Single shot echo planar imaging
STIR	Short tau inversion recovery
SUV	Standardized uptake ratio
V_e	Interstitial volume
VEGF	Vascular endothelial growth factor
VPCT	Volume perfusion CT

S.E. Rossi (✉)
Centro de Diagnóstico, Dr. Enrique Rossi,
Buenos Aires, Argentina
e-mail: santirossi@cdrossi.com

C. Trinidad
Department of Radiology, POVISA, Vigo, Spain

A. Luna, MD
Chief of MRI, Health Time Group, Jaén, Spain

Department of Radiology, University Hospitals,
Case Western Reserve University,
Cleveland, Ohio, USA
e-mail: aluna70@htime.org

29.1 Introduction

Lung cancer is a common malignancy and an estimated 228,190 new cases will be diagnosed in the USA in 2013 (*American Cancer Society* www.cancer.org). Imaging has an important role in the detection, diagnosis, and staging of the disease as well as in assessing response to therapy and monitoring for recurrence after treatment. This chapter will emphasize the appropriate use of positron emission tomography (PET-CT) in the management of patients with lung cancer and will briefly review new techniques that can be used to evaluate patients with lung cancer such as perfusion CT and functional MRI.

29.2 Diagnosis

Although the majority of patients with NSCLC present with advanced disease, a significant proportion of lung cancers manifest as a solitary pulmonary opacity [1]. Unfortunately, many benign and malignant opacities have similar morphologic features on conventional imaging and remain indeterminate after radiologic evaluation. However, FDG-PET-CT can be used to improve the characterization of focal pulmonary opacities as small as 7 mm [2–5]. FDG uptake can be assessed visually on PET images by comparing the activity of the lesion with that of the background or by semiquantitative

analysis using calculated standardized uptake values whereby the attenuation-corrected FDG uptake is normalized to the injected dose and the patient's body weight. Although a standardized uptake ratio of >2.5 is generally considered to be indicative of malignancy, a prospective trial in 585 patients (496 malignant and 89 benign nodules) showed that nodule with low SUV (<2.5) was associated with a 25 % likelihood of malignancy (Fig. 29.1). FDG-PET-CT has an overall sensitivity, specificity, and accuracy of 96, 88, and 93 % [6].

It is important to emphasize that the published data regarding FDG-PET evaluation of solitary pulmonary opacities indicating high sensitivity, specificity, and accuracy mostly pertains to nodules that are both solid and 1 cm or greater in diameter. Limitations in spatial resolution can result in false-negative studies when nodules smaller than 1 cm in diameter are evaluated [5, 7] Although there is little published data to determine the appropriate role of FDG-PET in the evaluation of nodules <1 cm in diameter, in general, because the resolution of PET scanners is in the order of 5 mm, FDG-PET-CT is not recommended in the routine evaluation of small nodules. In addition to the limitation of evaluating small nodules, FDG-PET also has low sensitivity for slow-growing neoplasms such as carcinoid tumors and subsolid nodules. In fact, on FDG-PET imaging, pulmonary carcinoid tumors usually have lower FDG uptake than expected for

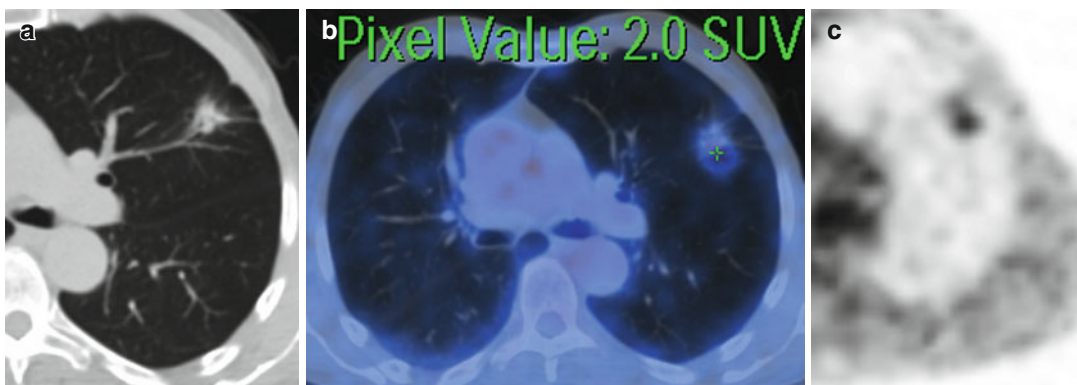
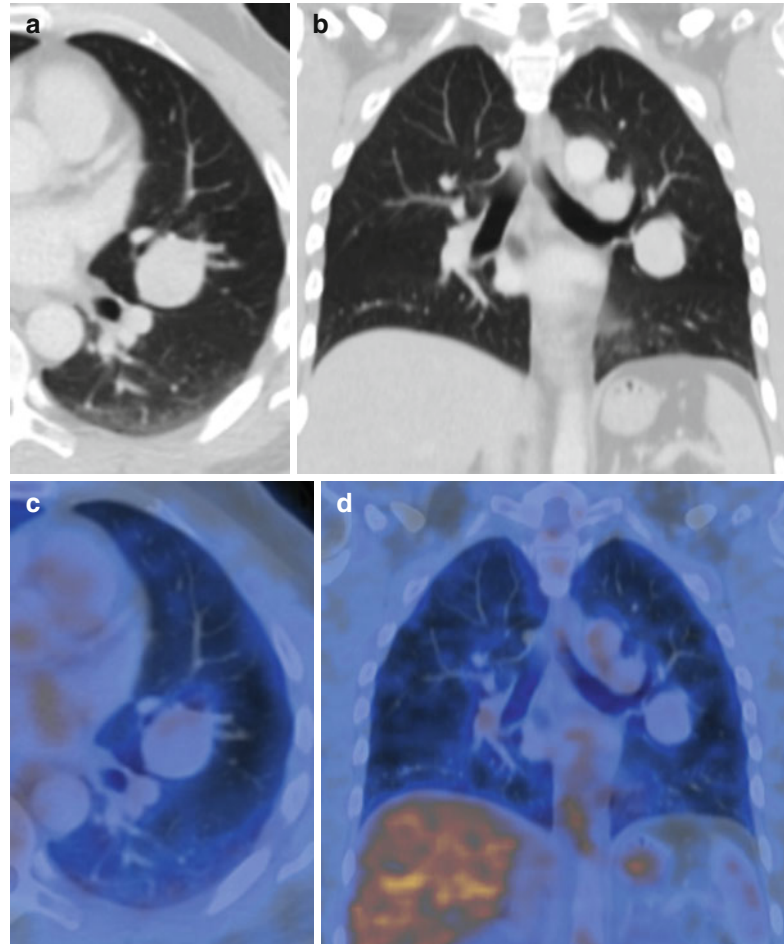


Fig. 29.1 A 64-year-old man with a primary lung adenocarcinoma. (a) CT shows a spiculated nodular opacity in the left upper lobe. (b, c) PET-CT image shows low FDG uptake within the nodule (SUV 2)

Fig. 29.2 A 40-year-old man with pulmonary carcinoid tumor. (a, b) Axial and coronal CT shows a well-defined pulmonary nodule (2.6 cm), in the left upper lobe. (c, d) PET-CT image shows no FDG uptake within nodule



malignant tumors (Fig. 29.2). Additionally, PET sensitivity is poor in the evaluation of NSCLC manifesting as subsolid nodules, particularly ground-glass opacities (GGOs) which can be due to atypical adenomatous hyperplasia, adenocarcinoma in situ (previously bronchioloalveolar carcinoma), and minimally invasive adenocarcinoma (previously adenocarcinoma with a predominant bronchioloalveolar component) due to a paucity (Figs. 29.3 and 29.4) [8, 9]. In terms of GGOs, Nomori et al. have reported a sensitivity of 10 % and specificity of 20 % (compared to 90 and 71 %, respectively, for solid nodules in the same study), i.e., nine of ten well-differentiated adenocarcinomas manifesting as ground-glass nodular opacities were falsely negative on

FDG-PET, while four of five benign ground-glass nodular opacities were falsely positive [7]. However, a review by Godoy and Naidich recommended that PET-CT could be warranted in GGOs with a mixed solid component as they represent a greater likelihood of being an invasive malignancy [10]. They postulate that the lower uptake of FDG in adenocarcinomas with bronchioloalveolar features may be of value in differentiating these malignancies from mixed subtypes of adenocarcinoma (Figs. 29.4 and 29.5). In this regard, the greater the FDG uptake, the greater the correlation with worse survival, while low uptake is associated with an indolent nature, lack of intratumoral lymphatic invasion, and nodal metastasis [10].

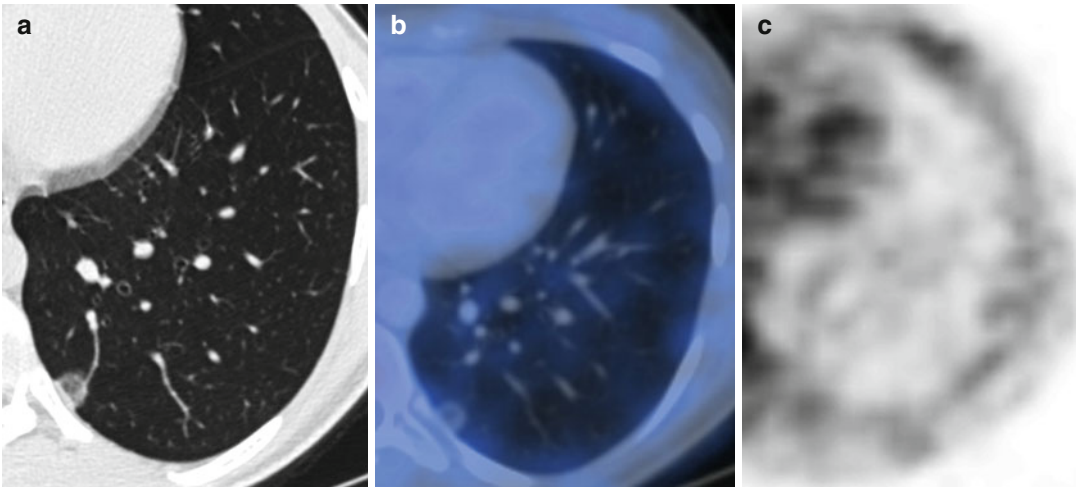


Fig. 29.3 A 60-year-old woman with a primary lung adenocarcinoma. **(a)** CT shows a pure ground-glass nodular opacity (GGO) in the left lower lobe. **(b, c)** PET-CT image shows no FDG uptake within the GGO. Note

although uncommon, adenocarcinomas manifesting as a small, pure GGOs commonly have no invasive component on histology and typically have low FDG uptake

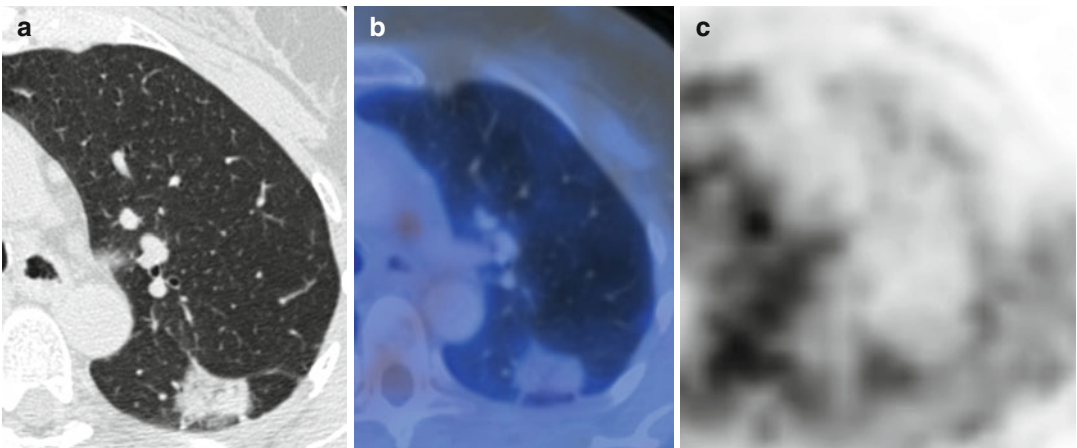


Fig. 29.4 A 66-year-old woman with a primary lung adenocarcinoma. **(a)** CT shows a pulmonary subsolid nodule with mixed ground-glass and solid attenuation

(2.5 cm), in the left lower lobe. **(b, c)** PET-CT image shows no FDG uptake within the nodule

29.3 Staging

The treatment and prognosis of patients with NSCLC depends on staging.

Patients with NSCLC are typically staged prior to therapy according to the recommendations of the International Staging System for Lung Cancer [11]. This system describes the

extent of NSCLC in terms of the primary tumor (T descriptor), lymph nodes (N descriptor), and metastases (M descriptor). The T descriptor is more optimally assessed by CT than PET due to the inherent poor resolution of PET scanners. In terms of the N and M descriptors, imaging is usually directed at detecting non-resectable disease, particularly contralateral hilar/mediastinal and supraclavicular nodal

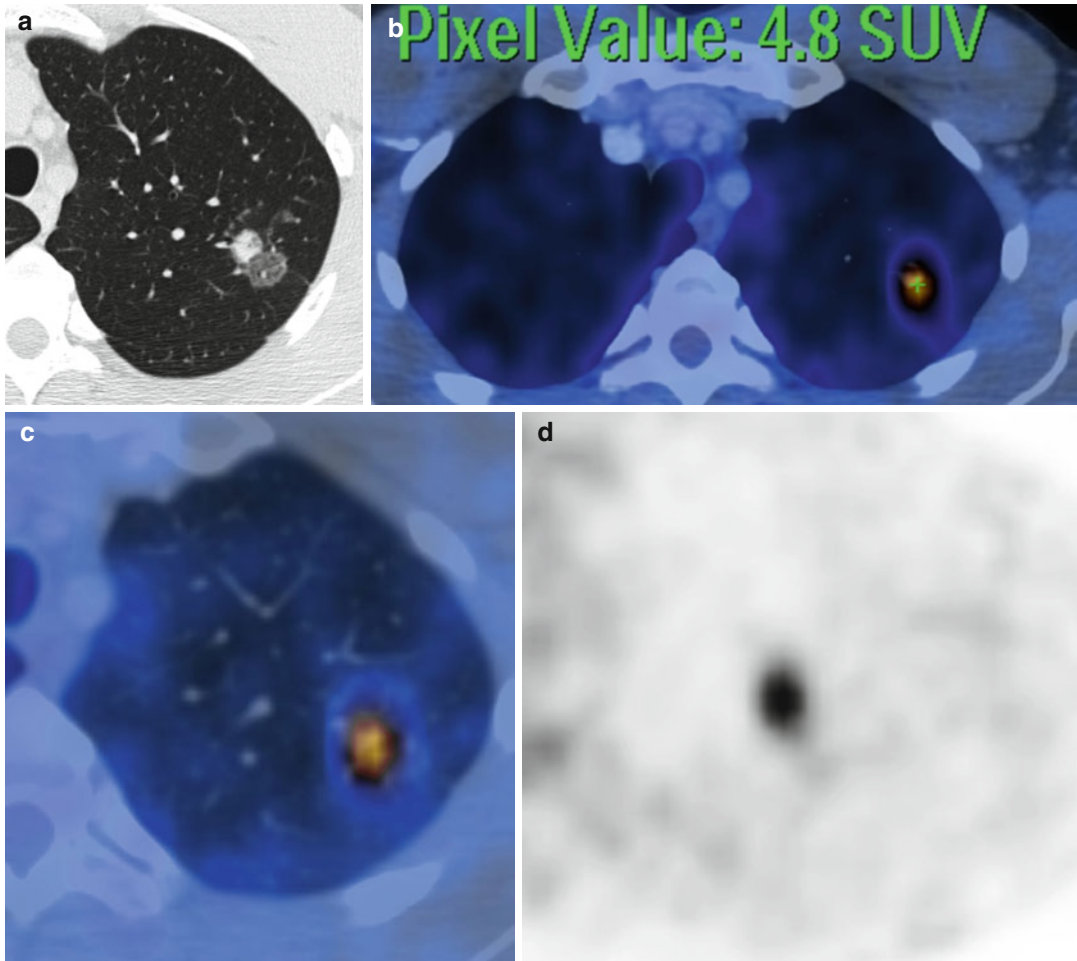


Fig. 29.5 A 67-year-old woman with a primary lung adenocarcinoma. (a) CT shows a pulmonary subsolid nodule with mixed ground-glass and solid attenuation (partially solid) (2.7 cm), in the left upper lobe. (b, c, d) PET-CT image shows FDG uptake within the solid component

of the nodule with an SUV of 4.8. Note that the GGO area shows no FDG uptake. Note the likelihood of invasive adenocarcinoma is high with mixed ground-glass and solid opacities, especially when the soft-tissue component is greater than two-thirds of the nodule

metastases and distant metastases (N3 and M1, respectively). The detection of N3 and/or M1 is important as these typically preclude surgical resection or require additional chemotherapy or radiotherapy. Whole-body FDG-PET is an important component of NSCLC staging, particularly in patients considered to be potentially resectable, as it improves the detection of nodal and distant metastases in patients staged with CT and frequently alters patient management [12–17].

29.3.1 Regional Lymph Nodes

The presence and location of nodal metastasis are of major importance in determining management and prognosis in patients with NSCLC [18]. CT is almost uniformly used to evaluate hila and mediastinal lymph nodes. Size is the only criterion used to diagnose nodal metastases, with nodes greater than 1 cm in short-axis diameter considered abnormal. However, lymph node size is not a reliable parameter for the evaluation of

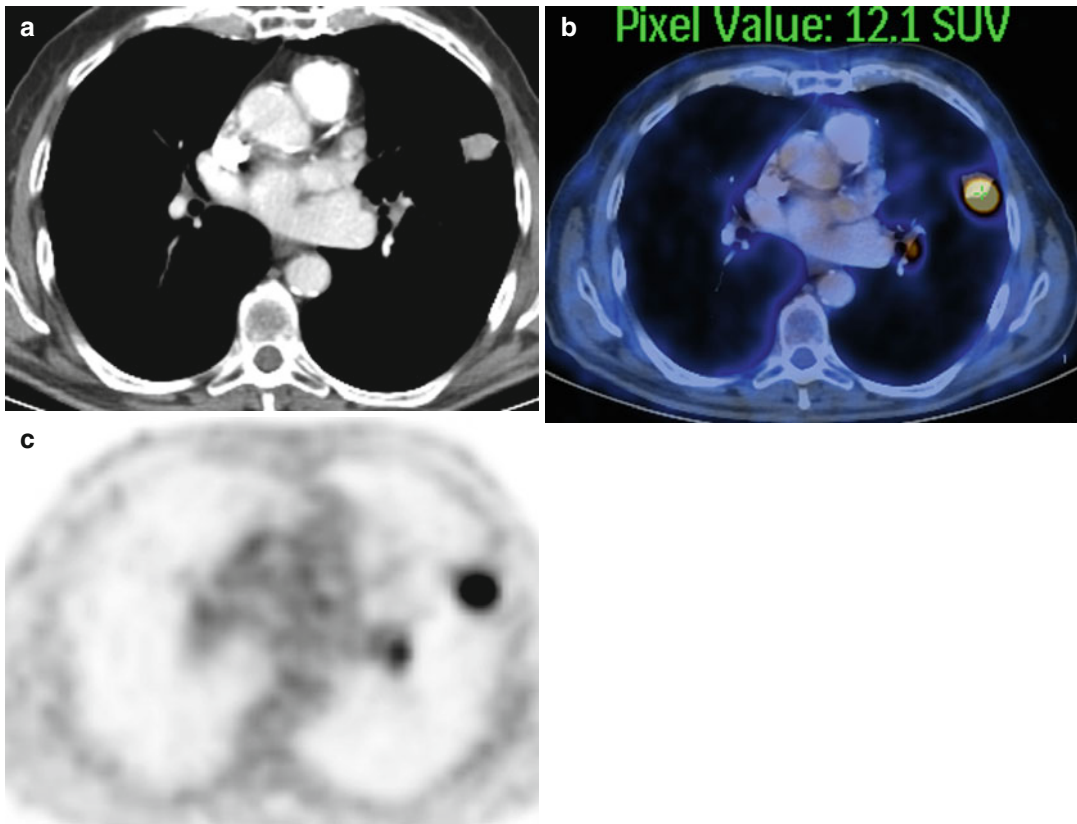


Fig. 29.6 A 58-year-old man with primary lung adenocarcinoma. **(a)** Contrast-enhanced CT shows a pulmonary nodule (2 cm) in the left upper lobe and a less than 1 cm

ipsilateral hilar lymph node. **(b, c)** PET-CT image shows FDG uptake within nodule (SUV 12) and hilar lymph node

nodal metastatic disease in patients with NSCLC [19–21]. Because surgical resection and potential use of adjuvant therapy are dependent on the patient’s N descriptor, attempts have been made to improve the accuracy of detection of nodal metastases.

FDG-PET complements CT findings and provides information on locoregional nodal staging that impacts management [15, 22, 23]. In a meta-analysis comparing PET and CT in nodal staging in patients with NSCLC, the sensitivity and specificity of FDG-PET for detecting mediastinal lymph node metastases ranged from 66 to 100 % (overall 83 %) and 81–100 % (overall 92 %), respectively, compared to sensitivity and specificity of CT of 20–81 % (overall 59 %) and 44–100 % (overall 78 %), respectively [22] (Fig. 29.6). FDG-PET-CT should be considered in all patients without CT findings of distant metastasis regardless of the size of mediastinal nodes, to detect occult nodal metas-

tasis and direct nodal sampling [15, 24, 25]. It is important to emphasize that the number of false-positive FDG-PET results due to infectious or inflammatory etiologies is too high to preclude mediastinoscopy and mediastinoscopy should be performed when nodal metastases will have an impact on management [24, 26, 27] (Figs. 29.7, 29.8, 29.9, and 29.10). Additionally, mediastinoscopy should be performed when the results of CT and PET are not congruent [24].

29.3.2 Metastatic Disease

Distant metastases (M1b) occur in 11–36 % of patients with NSCLC at presentation, and metastases are commonly to the lung, adrenals, liver, brain, bones, and extrathoracic lymph nodes [28]. The M1 descriptor is subclassified into M1a (additional nodules in the contralateral lung) and M1b (distant metastases outside the lung and

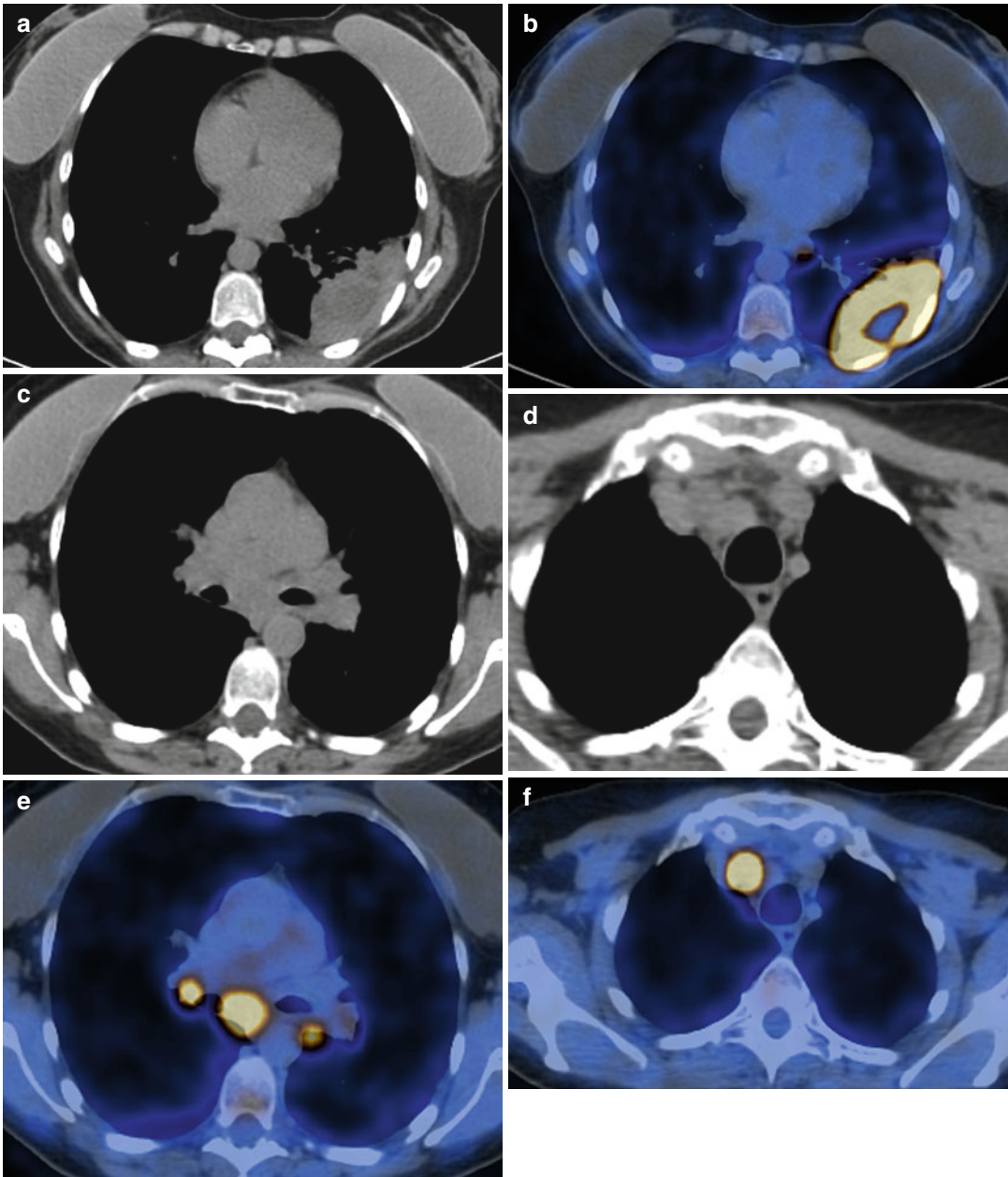


Fig. 29.7 A 68-year-old woman with primary lung adenocarcinoma. (a) CT shows a left lower lobe heterogeneous mass, contacting with the pleura. (b) PET-CT image shows FDG uptake within the mass with a central area with no FDG uptake (necrosis within the mass).

(c, d) Noncontrast CT (mediastinal window) shows left hilar, subcarinal, and right paratracheal adenopathy. (e, f) PET-CT image shows hilar (contralateral), subcarinal, and right paratracheal FDG uptake

pleura). CT is typically performed to detect M1 disease, but the accuracy is not optimal. Whole-body FDG-PET-CT is increasingly being used to improve the accuracy of staging. FDG-PET has a higher sensitivity and specificity than CT in detecting metastases to the adrenals, bones, and

extrathoracic lymph nodes and has been reported to have sensitivity, specificity, positive predictive value, and negative predictive value of 83, 90, 36, and 99 %, respectively, for M1 disease [15]. In fact whole-body PET-CT detects occult extrathoracic metastases in up to 24 % of patients

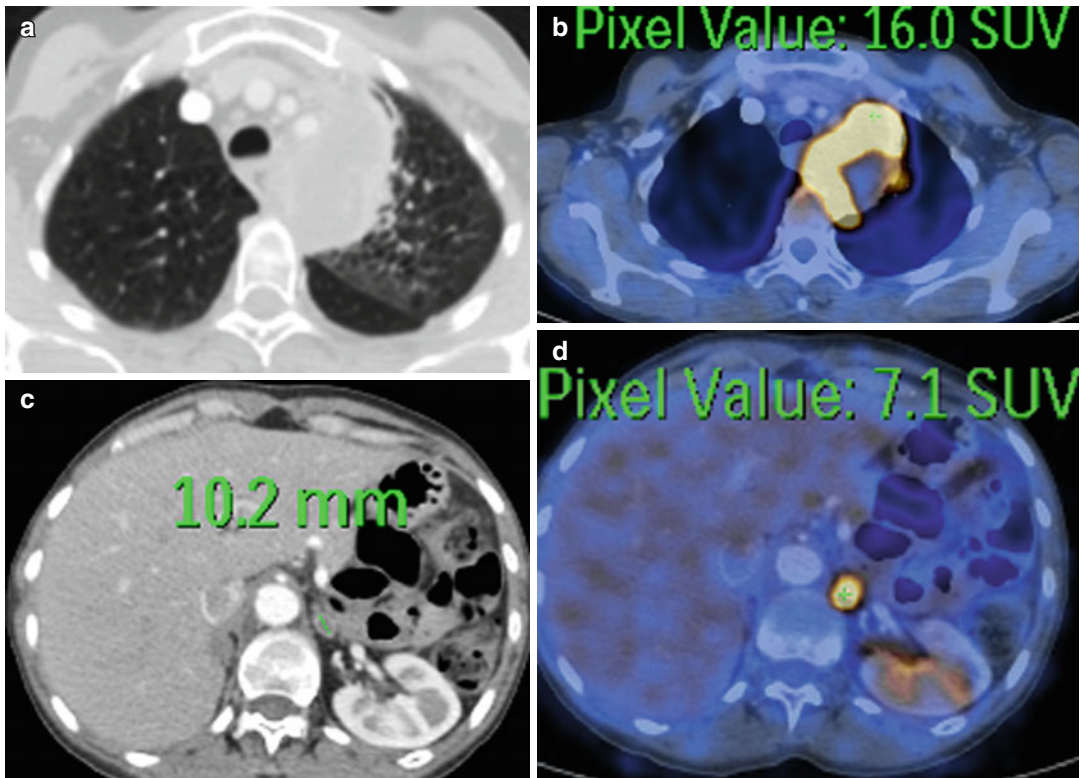


Fig. 29.8 A 70-year-old man with primary lung adenocarcinoma. (a) CT shows a left lower lobe heterogeneous mass, contacting with the mediastinal pleura. (b) PET-CT image shows FDG uptake within the mass (SUV 16). (c)

Contrast-enhanced CT enlargement of the left adrenal gland (1 cm). (d) PET-CT image shows FDG uptake of left adrenal gland (SUV 7). Biopsy confirmed adrenal metastases

selected for curative resection. In addition, the incidence of detection increases as the T and N descriptors increase, i.e., 7.5 % in early stage disease to 24 % in advanced disease, been shown to be cost-effective [12, 15, 17, 29, 30]. Two studies in patients being considered for surgical resection after standard clinical staging showed that FDG-PET prevented nontherapeutic surgery in one in five patients [15, 29].

29.4 Prognosis and Therapeutic Response

NSCLC commonly presents with advanced disease and chemotherapy is often important in the treatment of these patients. However, following initiation of chemotherapy, tumor progression can occur in up to one-third of patients [31]. FDG-PET-CT may allow an early and sensitive assessment of the effectiveness of anticancer chemotherapy as FDG

uptake is not only a function of proliferative activity but is also related to viable tumor cell number [32–35]. In NSCLC, use of SUV measurements has been shown to be as accurate and reproducible as more complex quantitative calculations based on dynamic imaging [33]. However, there is no clear consensus on when PET should be performed or the most appropriate criteria for assessment of tumor response by FDG-PET.

There have been a limited number of studies on the use of FDG-PET for determining prognosis and the monitoring of treatment response in patients with NSCLC. Preliminary studies suggest a possible role for PET as a prognostic marker with the degree of increased FDG uptake in the primary lesion at diagnosis related to survival rate [36–41]. The threshold SUV used for univariate analysis in these studies ranged from 3.3 to 20. In a recent study, disease-free survival of 98 patients with pathologic stage I adenocarcinoma who underwent curative

Fig. 29.9 A 65-year-old man with primary lung adenocarcinoma. (a) CT shows a left upper nodule. (b) Noncontrast CT shows bilateral enlargement of both adrenal glands. (c) PET-CT image shows no FDG uptake (adenomas)

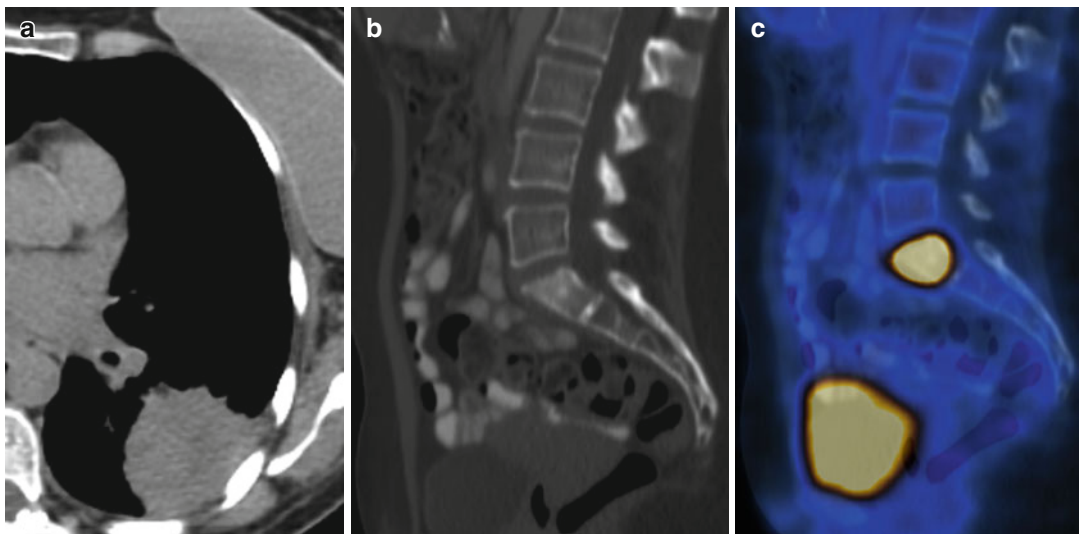
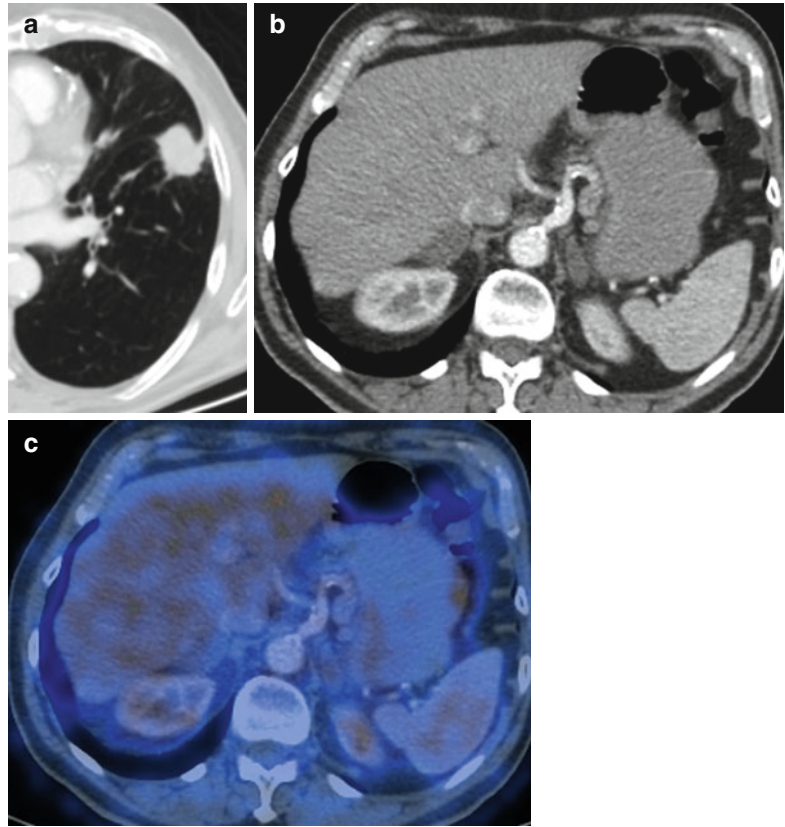


Fig. 29.10 A 55-year-old woman with primary lung adenocarcinoma. (a) CT shows a left lower heterogeneous mass. (b) Spine CT (bone window) shows sclerosis of S1

with no cortical disruption. (c) PET-CT image shows FDG uptake of S1. Bone biopsy confirmed metastases

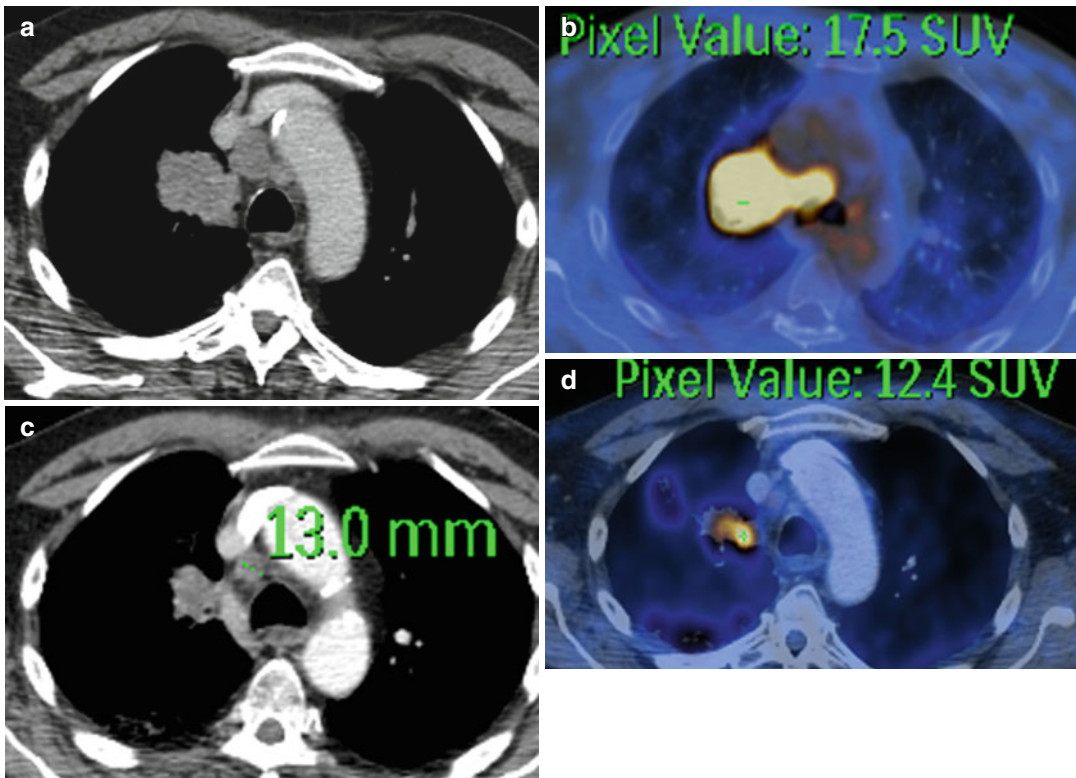


Fig. 29.11 A 63-year-old man with primary lung adenocarcinoma. (a, b) CT and PET-CT prior to therapy show marked increased FDG uptake by right upper lobe (SUV 17.5) and right superior paratracheal adenopathy. (c, d) CT and PET-CT after therapy show decrease in size

and FDG uptake of the mass (SUV 12.4). Note there is generally a significant association between marked decrease in FDG uptake within the primary tumor and patient outcome

resection was evaluated in relation to the SUV to determine the prognostic significance of FDG uptake on PET [41]. Twelve patients developed recurrence of malignancy after a mean post-resection period of 31 months. Ten (23 %) of the 43 patients with a SUV >3.3 developed recurrent disease compared with 2 (4 %) of the 55 patients with SUV <3.3 ($p = .020$). The authors concluded that FDG uptake appears to be predictive of disease-free survival and postulate that FDG-PET could be useful in determining the role of postoperative adjuvant chemotherapy in these patients.

Studies concerning treatment outcome and prognosis have usually investigated the use of FDG-PET following the completion of treatment (Fig. 29.11) [42–44]. In one such prospective study of the prognostic usefulness of FDG-PET following the completion of definitive

radiotherapy ($n = 10$) or chemoradiotherapy ($n = 63$) in 73 patients with unresectable NSCLC, the authors reported a significant association between the qualitative decrease in FDG uptake within the primary tumor and mediastinal lymph nodes and patient outcome and also confirmed previous observations of the superior prognostic value of FDG-PET compared to CT imaging following therapy [43].

FDG-PET has also been shown to be of value in patients with locally advanced but potentially resectable NSCLC who have completed neoadjuvant therapy, by identifying those who have had a pathological response to treatment and may benefit from further locoregional control [45–49]. In a prospective trial of 93 patients with NSCLC and biopsy-proven stage IIIA N2 disease, PET-CT was better than CT in evaluating

these patients after induction chemoradiation therapy. A decrease of 75 % in SUVmax of the primary tumor was highly indicative of a complete response, and a decrease by more than 50 % of the N2 node initially involved with metastatic cancer was highly indicative that there was no residual metastatic disease in the node [48].

There have been comparatively few studies assessing the value of early FDG-PET in assessing tumor response while patients are still receiving therapy [50, 51]. A decrease in FDG uptake before and after one cycle of chemotherapy may predict outcome with improved survival directly related to the magnitude of decreased uptake. In a prospective study of 47 patients with locally advanced but potentially resectable stage IIIA N2 NSCLC who were receiving neoadjuvant chemotherapy, a reevaluation FDG-PET performed after one cycle of induction chemotherapy showed that a decrease in FDG uptake ≥ 35 % or greater correlated with increased survival ($p=0.03$) [51].

In summary, FDG-PET may have an important role in the assessment of prognosis and therapeutic response. However, a limitation to widespread use and applicability is the lack of standardization of scanning methods and SUV measurements as well as lack of agreement on the optimal cutoff levels for determination of response. A consensus report by the Cancer Imaging Program of the National Cancer Institute states that FDG-PET can only be an important tool for assessing therapeutic efficiency in large multicenter trials after the application of standard protocols pertaining to patient preparation, image acquisition and reconstruction, PET timing relative to therapy, and image analysis [52]. More recently, Wahl et al. have proposed guidelines that are useful in standardizing the use of FDG-PET in the assessment of tumor response [53].

29.5 Recurrent Lung Cancer

In an attempt to prolong survival of patients with recurrent malignancy after attempted curative treatment of NSCLC, patients can be treated with repeat surgery, salvage chemotherapy, or radiotherapy [54–57]. Relying on patient

symptomatology to determine persistent or local recurrence of NSCLC can delay diagnosis and compromise retreatment. FDG-PET can detect local recurrence of tumor after definitive treatment with surgery, chemotherapy, or radiotherapy before conventional imaging and has been reported to have a sensitivity of 98–100 % and specificity of 62–92 % [58–61]. In one recent prospective study of 62 patients who had undergone surgical resection of NSCLC, PET was able to detect tumor recurrence (sensitivity 93 %, specificity 89 %, and accuracy 92 %) and predict which patients would benefit most from surgical retreatment [62].

In summary, PET compliments conventional radiologic assessment of NSCLC and is being routinely used to improve the detection of nodal and extrathoracic metastases. FDG-PET is also currently being evaluated in the assessment of prognosis and therapeutic response and by potentially allowing an earlier assessment of response may prove invaluable in the oncologic management of patients.

29.6 Functional MRI

29.6.1 Diffusion-Weighted MRI (DWI)

DWI has been explored in the evaluation of chest malignancies in the last decade. Shortcomings, such as motion artifacts related to breathing and heart and vascular pulsation and susceptibility artifacts associated with air-tissue interfaces, to a large extent preclude widespread application. However, recent technological improvements have overcome many of these limitations [63]. Currently an EPI sequence with spectral fat-suppression and parallel imaging is typically performed. In addition, different techniques of respiratory synchronization, such as breath-holding or respiratory trigger, are applied to avoid the macroscopic movement produced by the respiratory motion. However, because of time constraints, a cardiac trigger is usually only used when performing DWI in the chest when the lesion being evaluated is located immediately adjacent to the heart. Table 29.1 includes

Table 29.1 Technical parameters of chest DWI sequence

Single-shot spin-echo EPI
Phased-array surface coil
<i>b</i> values: 0, 100, 500, and 1,000 s/mm ²
FOV: 320–400
Parallel imaging acceleration factor of 2
Pixel resolution 2.5×2.5×7 mm ³
Spectral fat suppression
Number of slices 24
TR: 5,000 ms
TE: 53 ms (shortest)
Respiratory triggered
Three orthogonal motion-probing gradients

recommended technical parameters for chest DWI. Diffusion-weighted imaging with background tissue suppression (DWIBS) is a DWI sequence, using STIR as fat-suppression technique, usually used in whole-body MRI studies, and has also been tested in the lung and mediastinum. DWI of the chest is now feasible in 1.5T and 3T magnets, with similar performance [64].

At least two *b* values are needed to perform ADC quantification, which is mandatory in the evaluation of pulmonary or mediastinal lesions. More complex methods of evaluation of diffusion signal decay, such as Intravoxel Incoherent Motion (IVIM), are also being investigated in the chest [65].

29.6.1.1 Clinical Applications

Detection of Pulmonary Nodule

DWI performs reasonably well in the detection of pulmonary nodules with size over 5 mm compared to multidetector CT [66]. DWIBS has demonstrated similar accuracy and sensitivity to PET-CT in detection of pulmonary metastases with similar rates of false-positive lesions [67–69]. Noninvasive adenocarcinomas and metastasis smaller than 1 cm may produce false-negative results in both PET and DWI [70–73].

Pulmonary Nodule Characterization

Malignant pulmonary lesions usually show higher signal on high *b* value DWI acquisitions and lower ADC values than benign ones, due to increased cellularity, higher tissue disorganization, and increased extracellular space tortuosity. DWI has shown promising results in the

differentiation between benign (Fig. 29.12) and malignant nodules (Fig. 29.13). However, the comparison of results between series is limited due to lack of standardization in technical parameters, post-processing, and evaluation method. Using threshold ADC values between 1.1 and 1.4×10⁻³ mm²/s, pooled sensitivities between 70 and 90 % and specificities between 74 and 100 % have been reported [65, 74]. Furthermore, a recent meta-analysis of the diagnostic performance of DWI in this task indicated a pooled sensitivity of 80 % and specificity of 93 %, with an AUC of 0.91 [75]. In general, DWI performs equivalently to PET in pulmonary lesion characterization, with similar limitations, although DWI tends to have less false-positives. False-positives on DWI are related to benign inflammatory lesions, and potential false-negatives are low-grade adenocarcinomas and metastasis.

Lung Cancer

DWI may be useful in distinction between lung cancer types. In this sense, small cell lung cancer (SCLC) has demonstrated statistically significant lower ADC values than non-small cell lung cancer (NSCLC) [72]. In addition, DWI may help in noninvasive assessment of histological grading of lung cancer. Several series have shown significant higher ADC values in well-differentiated adenocarcinomas compared to more aggressive adenocarcinomas or [76], squamous carcinomas [77]. Furthermore, DWI has been proposed to accurately evaluate tumor grade, mediastinal node stage, and degree of invasiveness [78, 79]. In addition, ADC has been proposed as a new prognostic marker in NSCLC, demonstrating a good correlation with tumor grade and with metastatic mediastinal nodes [79]. However, in the evaluation of adenocarcinomas, there are contradictory data about the capabilities of DWI in the detection of invasive histologic subtypes [71, 77].

Other applications of DWI in lung cancer evaluation include distinction of central lung cancer from postobstructive consolidation (Fig. 29.14) (an important distinction in radiotherapy planning), assessment of Pancoast tumors, post-treatment monitoring (Fig. 29.15), detection of recurrence, and prediction of treatment response

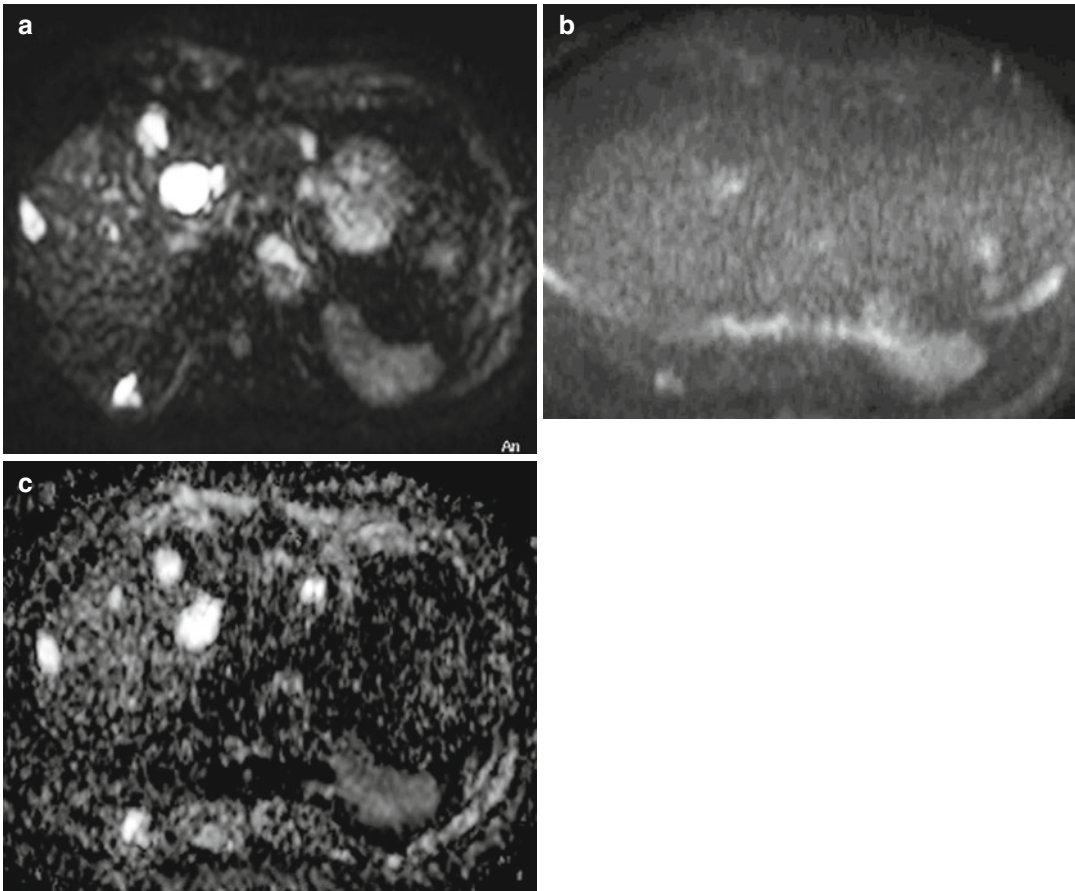


Fig. 29.12 A 75-year-old man presents an incidental nodule in right lower lobe. Chest MRI was performed for further assessment. SS EPI DWI with b values of 0 and 800 s/mm^2 (**a**, **b**) show disappearance with higher b values of a well-defined hyperintense nodule in peripheral loca-

tion of the right posterobasal segment, consistent with absence of restriction of diffusion as confirmed in the ADC map (**c**). The mean ADC value of the lesion was $2.3 \times 10^{-3} \text{ mm}^2/\text{s}$. Biopsy confirms inflammatory origin

[65, 83]. An increase in ADC have been related to good response to different types of treatment [80, 98]. Preliminary data suggest that changes in ADC as early as after one course of chemotherapy in advanced lung cancer can discriminate between responders and nonresponders in a similar manner to SUV increase. Furthermore, in the prediction of treatment response in lung cancer, significant different progression-free survival and overall survival between responders and nonresponders estimated by DWI have been reported [81, 99]. Similarly, Yabuuchi and colleagues demonstrated the superiority of ADC to DCE-MRI-derived parameters in the early assessment of response to chemotherapy of advanced NSCLC. In this series, there was

a significant correlation between early ADC changes and reduction in tumor size as well as an increase in the median progression-free survival in those with an increase in the ADC [82]. In addition, one series by Ohno and colleagues revealed a better prediction of response to chemoradiation of NSCLC patients using DWI than FDG-PET-CT. The AUC, specificity, and accuracy for the ADC were significantly larger than for SUV_{max} . [83]. Similarly, Okuma and colleagues demonstrated a significant early increase in ADC values of responding malignant lung lesions treated with CT-guided radio frequency [84, 102]. However, overall the prognostic value of pretreatment ADC in patients with lung cancer is unclear [80].

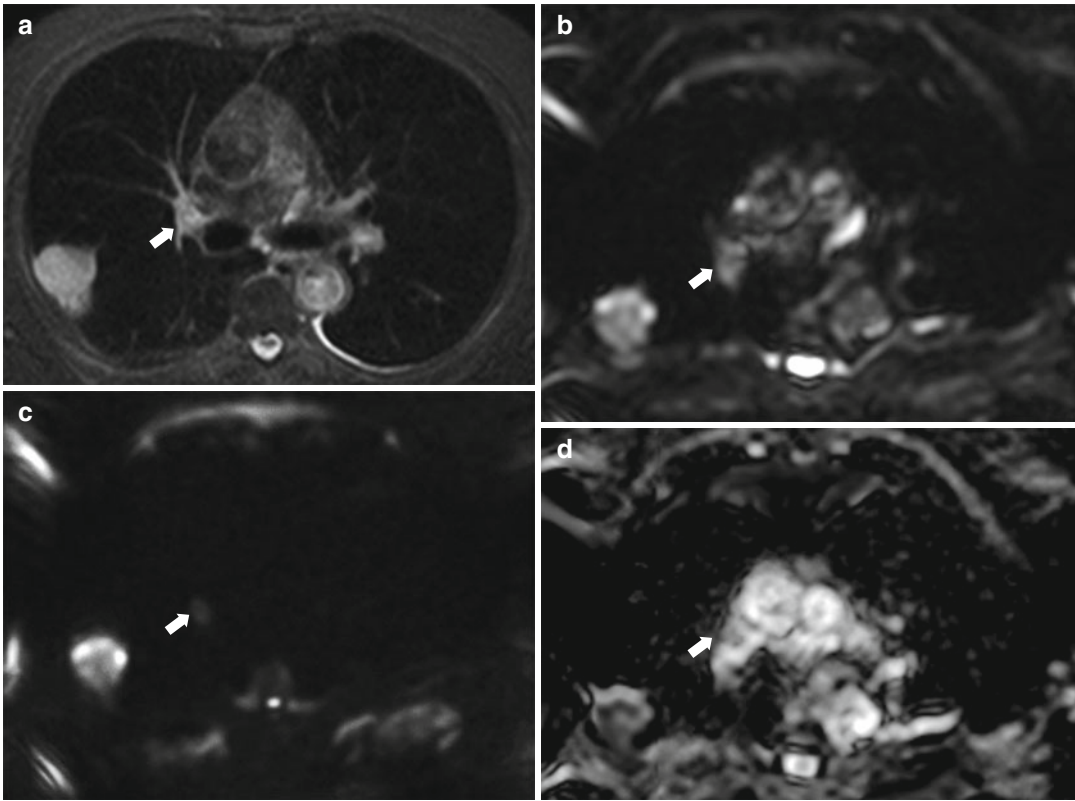


Fig. 29.13 A 63-year-old man presents with acute malignant collapse of L1 vertebral body. Whole-body MRI was performed searching for primary malignancy. (a) Axial black-blood STIR shows peripheral nodule in right lung and ipsilateral hilar lymph node (*arrow*). (b, c) Both lesions are hyperintense on DWI with b values of 0

and $1,000 \text{ s/mm}^2$. (d) Low signal intensity of both lesions on ADC map confirms restriction of diffusion, suggesting a malignant origin. Biopsy confirmed high-grade adenocarcinoma and metastatic hilar lymph node (*arrows* in all images)

Staging of NSCLC with DWI

Local staging (T staging) of NSCLC has not been extensively studied with DWI. However, DWI has shown promising results in the N staging [85, 86]. In this sense, Nomori and colleagues demonstrated, using a DWI sequence with respiratory trigger and spectral fat suppression, a significant increase in accuracy in the N staging of NSCLC compared to PET, mainly due to less over-staging [87]. Furthermore, an inverse correlation between ADC and standardized uptake value (SUV) on FDG-PET-CT has been recently reported [88]. Conversely, several series using a DWIBS sequence have achieved less accuracy than PET-CT in the N staging of lung cancer [70, 89]. Surprisingly, Ohno and colleagues have recently obtained more sensitive and/or more accurate assessment of N

stage disease in patients with NSCLC using STIR turbo SE MR imaging than with DWI and FDG-PET-CT [90]. A recent meta-analysis has proposed DWI as a reliable alternative to FDG-PET-CT for the preoperative staging of mediastinal and hilar lymph nodes in patients with NSCLC, demonstrating similar sensitivity and significant better specificity [91]. However, the combined interpretation of MRI and PET-CT enhances the detection of nodal metastasis in patients with NSCLC [92].

Whole-body DWI has also been proposed for M staging of NSCLC, with similar results to PET-CT (Fig. 29.16) [69, 70]. It is important to emphasize that whole-body DWI should be used along with morphological whole-body sequences in order to improve the diagnostic accuracy [69]. In the specific case of bone metastasis, whole-body DWI has

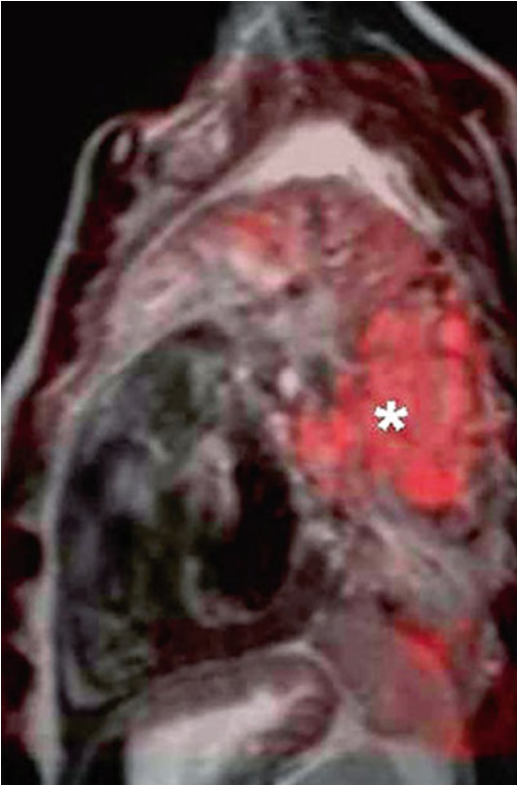


Fig. 29.14 Central squamous cell carcinoma with left lung atelectasis. Fusion imaging of sagittal TSE T2-weighted and DWI with a b value of $1,000 \text{ s/mm}^2$ at the same level allows accurate differentiation of the tumor borders (*asterisks*) from postobstructive pneumonitis. Notice how central tumor shows a greater degree of restriction than peripheral postobstructive pneumonitis

demonstrated better specificity and accuracy than scintigraphy or PET-CT [93].

29.6.2 Dynamic Contrast-Enhanced MRI (DCE-MRI)

DCE-MRI is noninvasive and is sensitive to tumor perfusion parameters such as vascular volume, vascular permeability, and flow. DCE-MRI is able to accurately distinguish between benign and malignant pulmonary nodules, with reported sensitivities ranging from 94 to 100 %, specificities from 70 to 96 %, and accuracies $>88 \%$ [94]. Furthermore, DCE-MRI has shown better specificity and accuracy than multidetector CT and co-registered PET-CT in the

differentiation between benign and malignant nodules [70].

DCE-MRI enables the angiogenesis of pulmonary nodules to be analyzed and also reflects the presence of other tissue components such as fibrosis, necrosis, or scarring. However, its clinical implementation has been limited due to difficulties to implement a robust and clinically useful technique. Movement artifacts are an important limitation and require the use of correction motion software. Visual assessment of enhancement pattern, morphology of time intensity curve, or derived parametric maps are useful in differentiating between malignant and inflammatory lesions although an overlap is present in the patterns of enhancement (Fig. 29.17) [94, 95]. Currently, DCE-MRI is used as a problem-solving modality in clinical practice, especially in cases where CT or PET-CT results are inconclusive. The opportunity to combine DCE-MRI in the same protocol as morphological STIR, T2-weighted and T1-weighted sequences, and functional DWI makes chest MRI a powerful tool to assess lung cancer. Most commonly, 2D or 3D GE sequences are repeated during several breath holds in a 5-min period of time, which allows an assessment of washout. As it is necessary a high temporal resolution, limited coverage, and the use of parallel imaging are necessary.

The role of DCE-MRI in the monitoring of NSCLC treatment has also been investigated. Ohno and colleagues demonstrated that parameters derived from a monocompartmental model of analysis of DCE-MRI, such as the maximum relative enhancement ratio and the slope of enhancement, were significantly lower in the local control group of patients with NSCLC treated with chemoradiotherapy than those in the local failure group [96]. In addition, there was a significant difference between the mean survival periods of both groups.

Ultimately, several series have evaluated DCE-MRI in the early assessment of NSCLC treated with anti-angiogenic drugs. Since the advent of this novel treatment, bicompartamental analysis of DCE-MRI has been used, as derived parameters such as K^{trans} and K^{ep} are better imaging biomarkers of tumor angiogenesis than those derived from

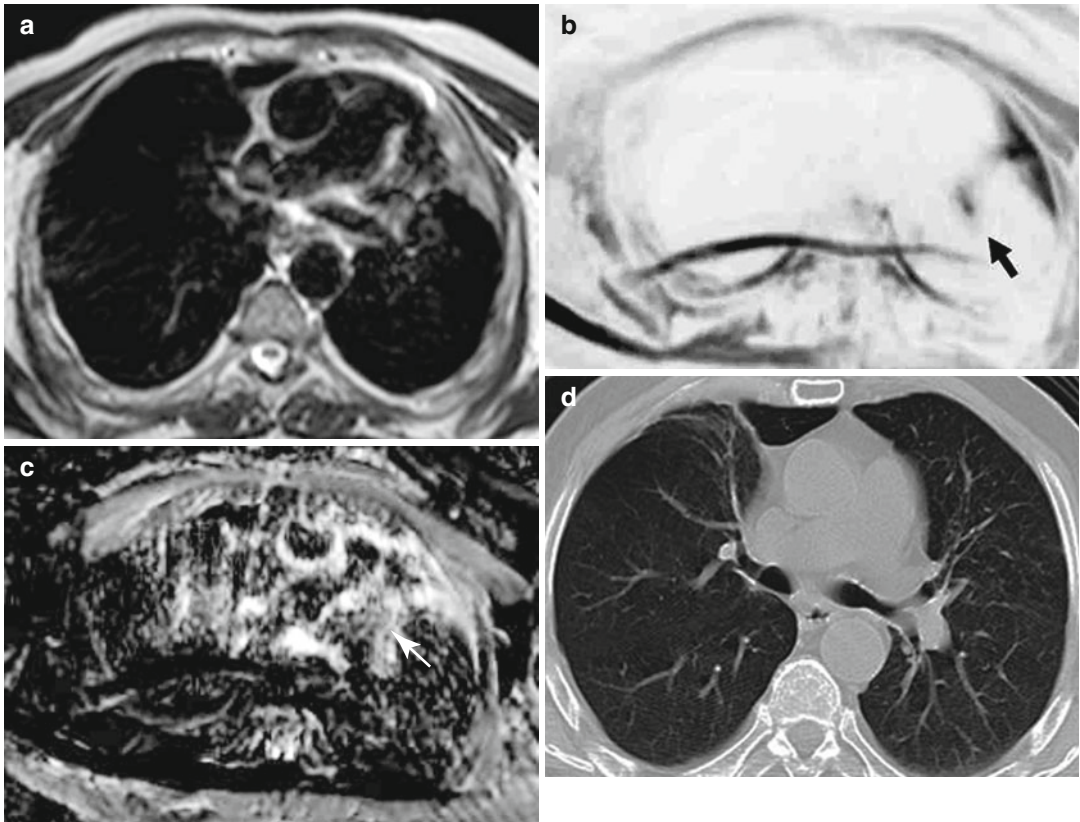


Fig. 29.15 A 62-year-old man, smoker (30 pack/year) presents with partial atelectasis of left superior lobe on chest radiograph. On chest CT, a central mass was suspected although it was difficult to depict. Bronchoscopy confirmed a low-grade adenocarcinoma. Chest MRI was performed for staging purposes. (a) Axial TSE T2-weighted image shows collapse of the apical segment of the left superior lobe, although the mass is difficult to

identify. However, a low-intensity hilar lesion (*arrow*) is identified on DWI image with a b value of $1,000 \text{ s/mm}^2$ and inverted grayscale (b). A mean ADC value of $1.9 \times 10^{-3} \text{ mm}^2/\text{s}$ (c) is consistent with the tumor histology of low-grade adenocarcinoma (*arrow*). CT performed 3 months after chemotherapy (d) showed complete remission of the lesion and disappearance of the atelectasis

a semiquantitative or monocompartmental model (see Chaps. 8 and 16). In this sense, Kelly and colleagues have shown that K^{ep} has a significant predictive value for overall survival and progression-free survival in patients with stage IV NSCLC treated with sorafenib [97]. Similarly, Chang et al. demonstrated a significant early decrease of mean and standard deviation of the K^{trans} histogram as well as a decrease of mean of the K^{ep} histogram in responders to anti-angiogenic agent bevacizumab combined with gemcitabine and cisplatin. Furthermore, NSCLCs with larger mean values of K^{ep} and smaller standard deviation of V_e on histograms before chemotherapy were considered predictors for treatment response

[98]. However, another series has shown that PET-CT is a better predictive test than DCE-MRI for progression-free survival in the early response evaluation of stage IIIb/IV NSCLC treated with bevacizumab and erlotinib [99]. Accordingly, the promising results of DCE-MRI in the early post-treatment monitoring and prediction of treatment outcome need to be validated with multicentric studies.

In summary, clinical applications of DWI of the chest have been limited by susceptibility and motion artifacts. Improvements in gradient strength, parallel imaging, and synchronization have recently allowed its use in lung nodule characterization, lung cancer evaluation, and

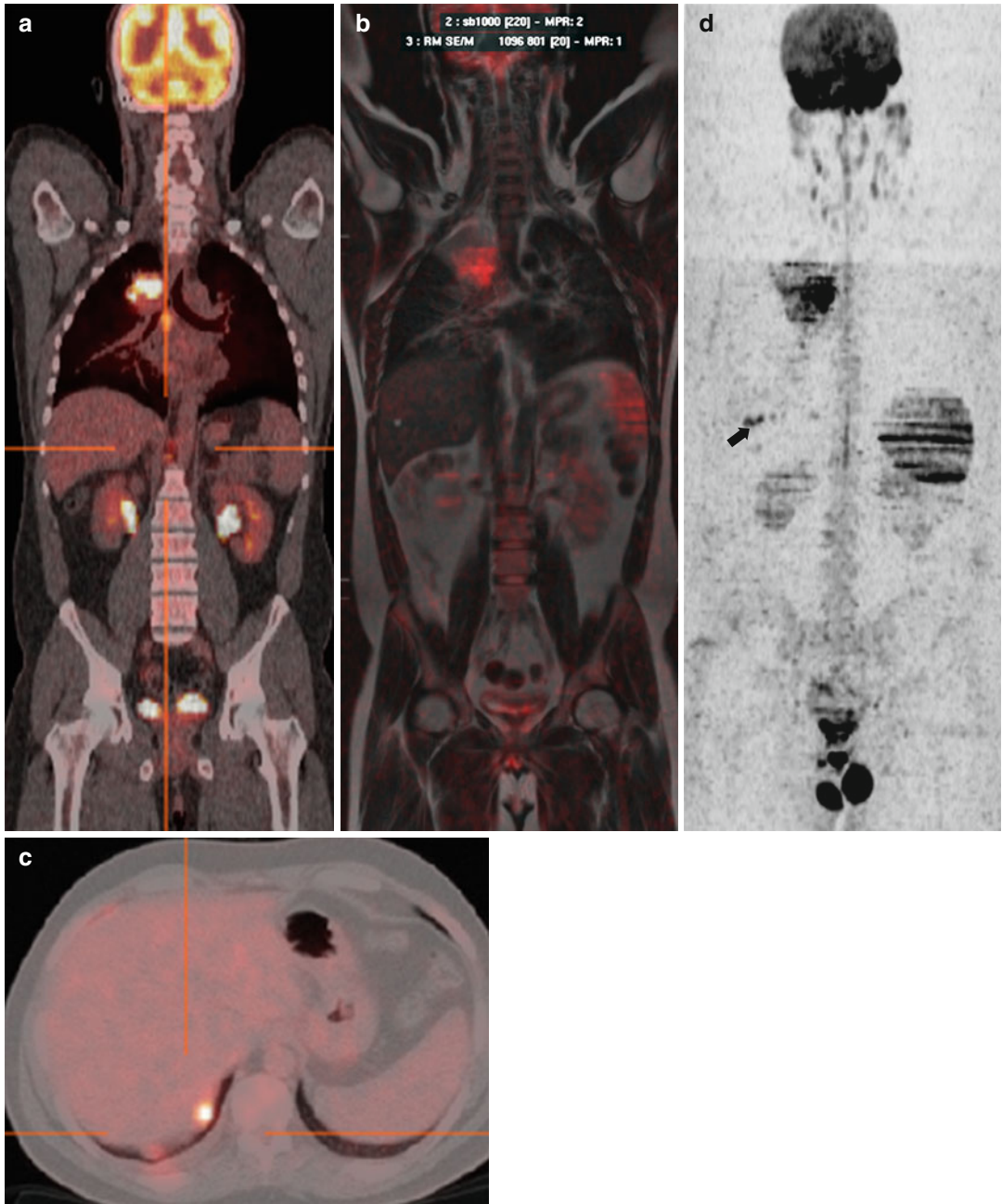


Fig. 29.16 Lung adenocarcinoma staging with both 18-FDG-PET-CT (a, c) and whole-body diffusion (b, d) shows both right superior hilar mass (a, b) and small right basal pleural implants (arrow, c, d)

investigation of mediastinum, pleura, and chest wall. In addition, DCE-MRI is useful in the distinction of benign and malignant tumors and has shown a promising role in the posttreatment monitoring and prediction of treatment

outcome of patients with NSCLC treated with chemoradiation or novel drugs. Due to technical difficulties, the use of DCE-MRI in clinical practice has been limited. MRI protocols including these two functional approaches along with

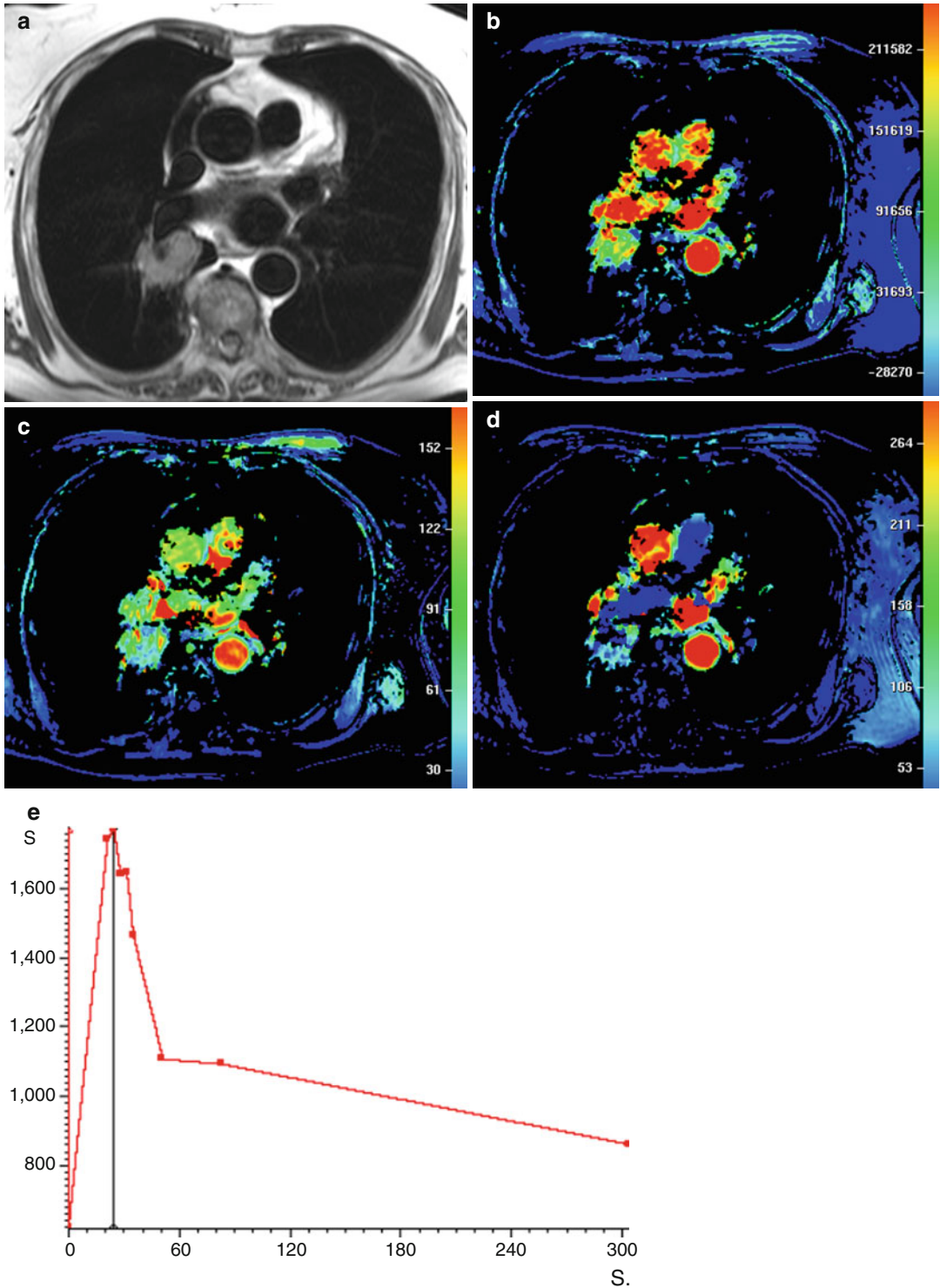


Fig. 29.17 An 81-year-old woman presented with hemoptysis. Bronchoscopy demonstrated a pulsatile mass causing obstruction of right B1 bronchi. Biopsy could not be performed due to risk of hemorrhage. (a) Axial black-blood T1-weighted sequence confirms right hilar mass.

(b, c, d) AUC, wash-in and washout parametric maps derived of DCE-MRI show the hypervascular nature of the mass. (e) Time intensity course of the mass typical for malignancy

morphological sequences are very attractive in the evaluation of lung cancer, although validation in the clinical arena is required.

29.7 Perfusion CT

Volume perfusion CT (VPCT) is a reproducible technique displaying high inter- and intraobserver agreement [100, 101]. Preliminary studies have suggested its potential role as prognostic biomarker and in the assessment of monitoring response to treatment of lung cancer. Bearing in mind that CT is the technique of choice for staging and monitoring patients with lung cancer, a change in protocols to introduce perfusion studies is appealing and relatively simple. A significant correlation with microvessel density (MVD) has been found for some perfusion parameters like blood flow (BF) (0.71), permeability (PMB) (0.68), and blood volume (BV) (0.76) in patients with NSCLC [102, 103]. A relationship has also been described between BV/PMB and immunohistochemical markers of tumor hypoxia [104].

29.7.1 Technique

Assessment of lung tumors with VPCT is challenging due to respiratory movement artifacts and limitations in acquisition secondary to breath-hold time, and this is especially important in small peripheral tumors. Accordingly, VPCT should normally not be performed in the evaluation of tumors smaller than 2 cm in diameter.

It is important to emphasize that the mathematical model used for obtaining perfusion parameters determines the acquisition technique for the study. To date, there are no standard measurements, and the available post-processing software use different mathematical approaches. In addition, there is no agreement on the optimum contrast dose, time, and injection protocol. It is important to reduce the radiation dose as much as possible by adjusting the scanner range to the tumor volume and using low kilovoltage. The intervals between scans (temporal resolution) must be below 1–1.5 s.

29.7.1.1 Post-processing

Automatic algorithms for three-dimensional movement correction and noise correction are applied. Movement is corrected with regard to the tumor center. The complete tumor volume is isolated avoiding lymphangitis, pneumonitis, atelectasis, or peritumoral areas of fibrosis, because the perfusion values in these lesions are often superimposed on those of the tumor, so that it is impossible to distinguish them. The definition of density thresholds between –50 and 150 HU, for the inferior and superior limits, respectively, excludes lung parenchyma and normal vascular structures from the analysis, even if they are inside the volume of interest (Fig. 29.18). In addition, parametric color maps and numerical measures expressed in average and typical deviation for each of the perfusion parameters are automatically generated. Those used commonly are BF, BV, PMB, or K^{trans} and mean transit time (MTT). A tumor time-density curve is also obtained and used for interpreting the results (Fig. 29.19).

29.7.2 Clinical Applications

29.7.2.1 Characterization of Lesions

Although some studies have shown that VPCT can be more specific and safer than PET-CT [105] for differentiating benign and malignant nodules, the variability of perfusion parameters is high, and overlapping of tumor and inflammatory lesions occurs. According to published data, it is not possible to confidently distinguish benign and malignant lesions on the basis of perfusion features alone. In addition, to date, perfusion values have not been useful in determining the histological type or differentiating small cell from NSCLC. The utility for distinguishing metastatic from non-metastatic nodes in lung cancer has also not been studied, and currently VPCT is not used clinically in the characterization or the staging of tumors.

29.7.2.2 Pretreatment Study of the Tumor

Most of published studies have found significantly higher perfusion values in the early stages of the

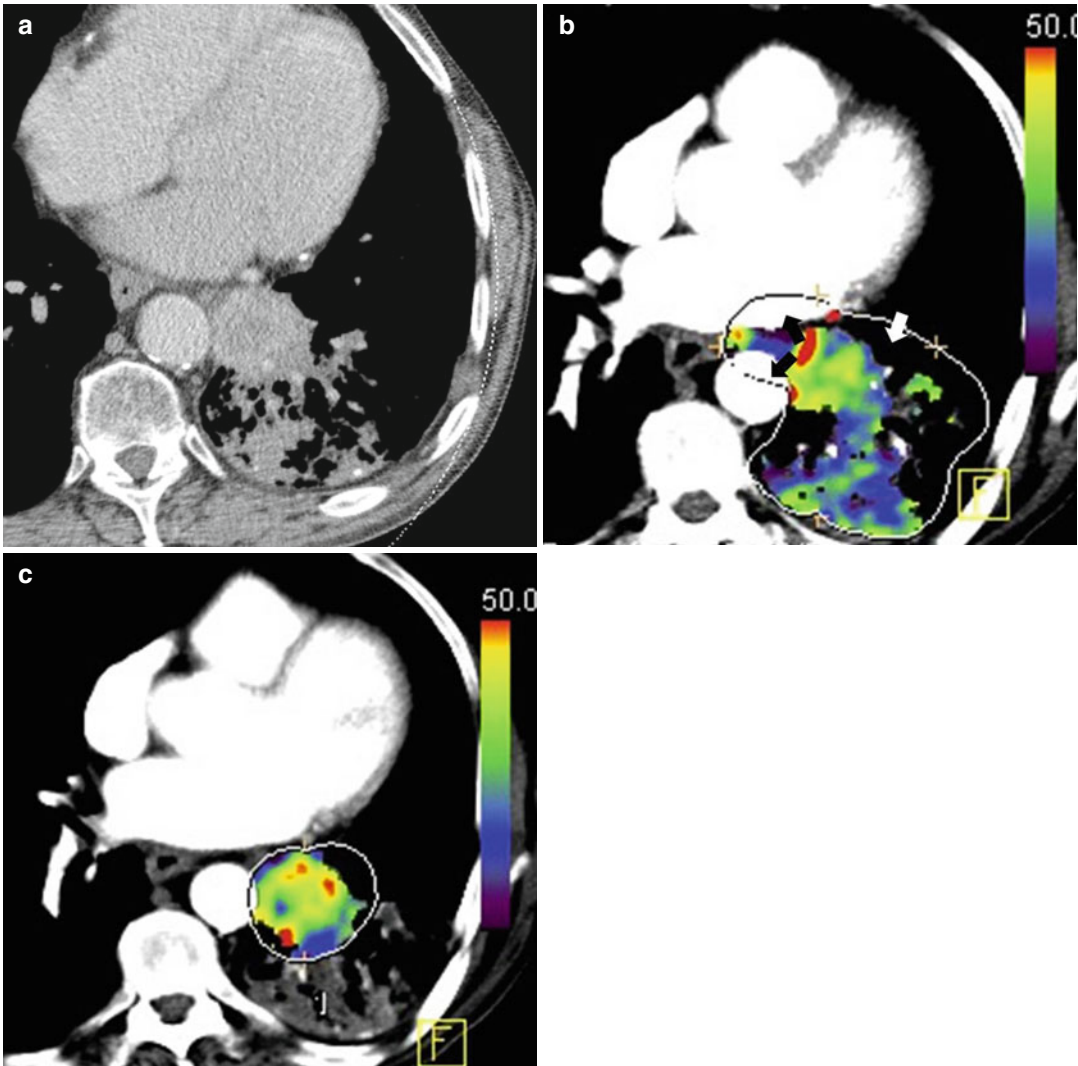


Fig. 29.18 (a) Axial noncontrast CT shows a lung mass with postobstructive pneumonitis. (b) Density thresholds exclude normal lung parenchyma (*white arrow*) and vascular structures (*black arrows*) included in the volume of

interest (*line*) from the analysis but not the area of pneumonitis which should be excluded from segmentation to avoid misinterpretation (c)

disease. Furthermore, some series have shown higher BF and PMB values in good responders to treatment [10, 106]. Therefore, VPCT might provide information with prognostic value, such as prediction of survival or response to treatment.

29.7.2.3 Treatment Monitorization

When anti-angiogenic therapy is used, VPCT may detect early changes in tumor vascularization, which may help to predict therapeutic

response before tumor size decreases. There are two studies showing a significant early reduction of BF and PMB parameters in NSCLC patients under anti-angiogenic therapy with bevacizumab and anti-VEGF (vascular endothelial growth factor) drugs [107, 108].

Further research is needed to determine the ability of VPCT to detect an early response after treatment with conventional chemotherapy. The studies published to date have demonstrated changes in

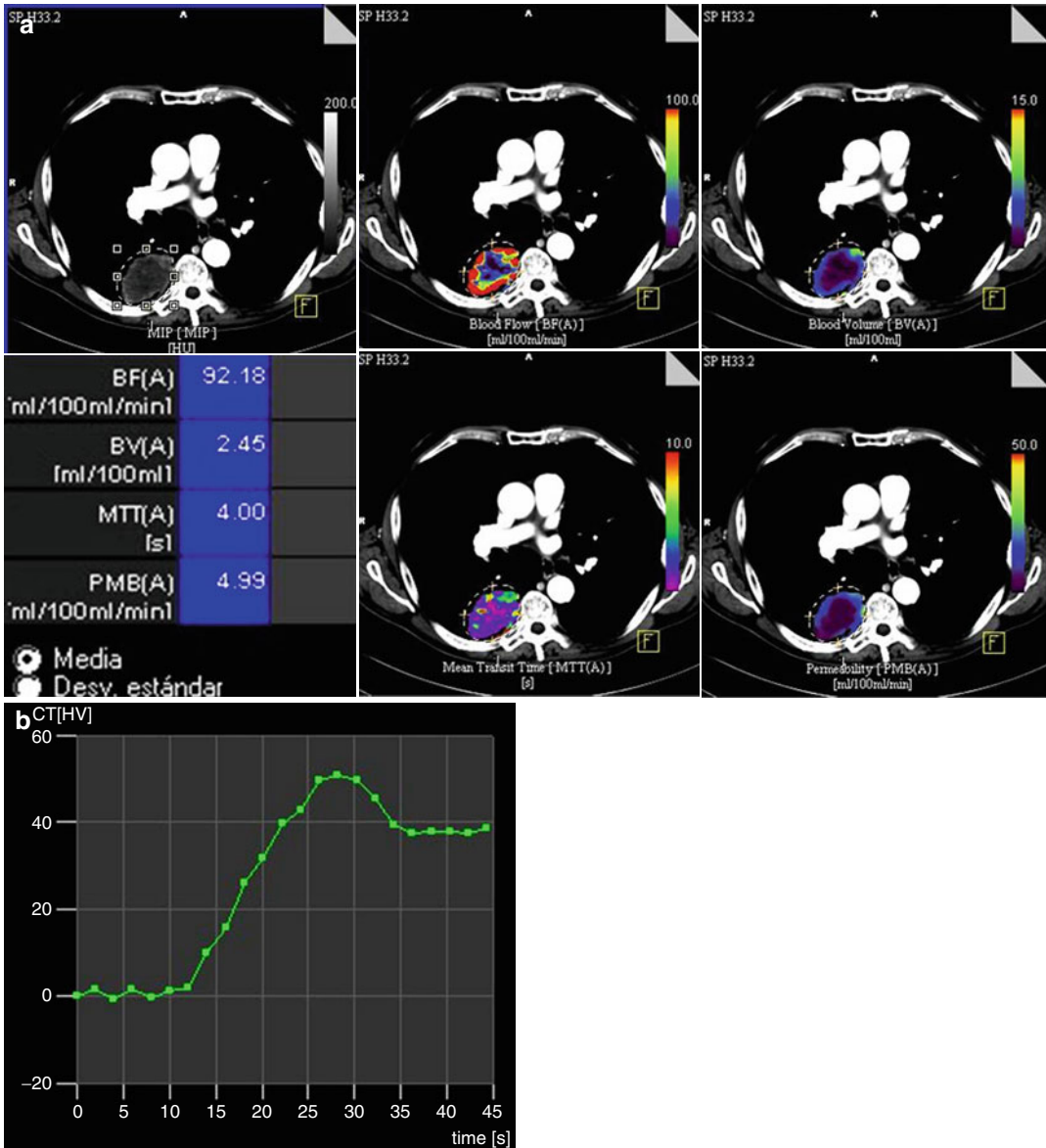


Fig. 29.19 (a) Right lower lobe mass with central necrosis. Parametric color map and numerical measurement expressed in average and typical deviation for each of the

perfusion parameters. Central necrosis correlates well with the color maps. (b) Tumor time-density curve with a morphology typical for lung cancer

perfusion parameters which, in most of the cases, are not significantly correlated with response to treatment. However, significant decreases in BF, BV, and PMB have been reported after treatment with radiotherapy (RT) [106] (Fig. 29.20).

A basal perfusion study must always be performed before treatment. Follow-up VPCT can be completed in the same session as routine

control CT. The optimal time interval has not been defined, but it is clear that it has to be determined individually for each drug type. However, VPCT should never be performed within the first 2 weeks after finishing RT, since an increase in the perfusion values has been observed due to a temporary inflammatory reaction related to cell death.

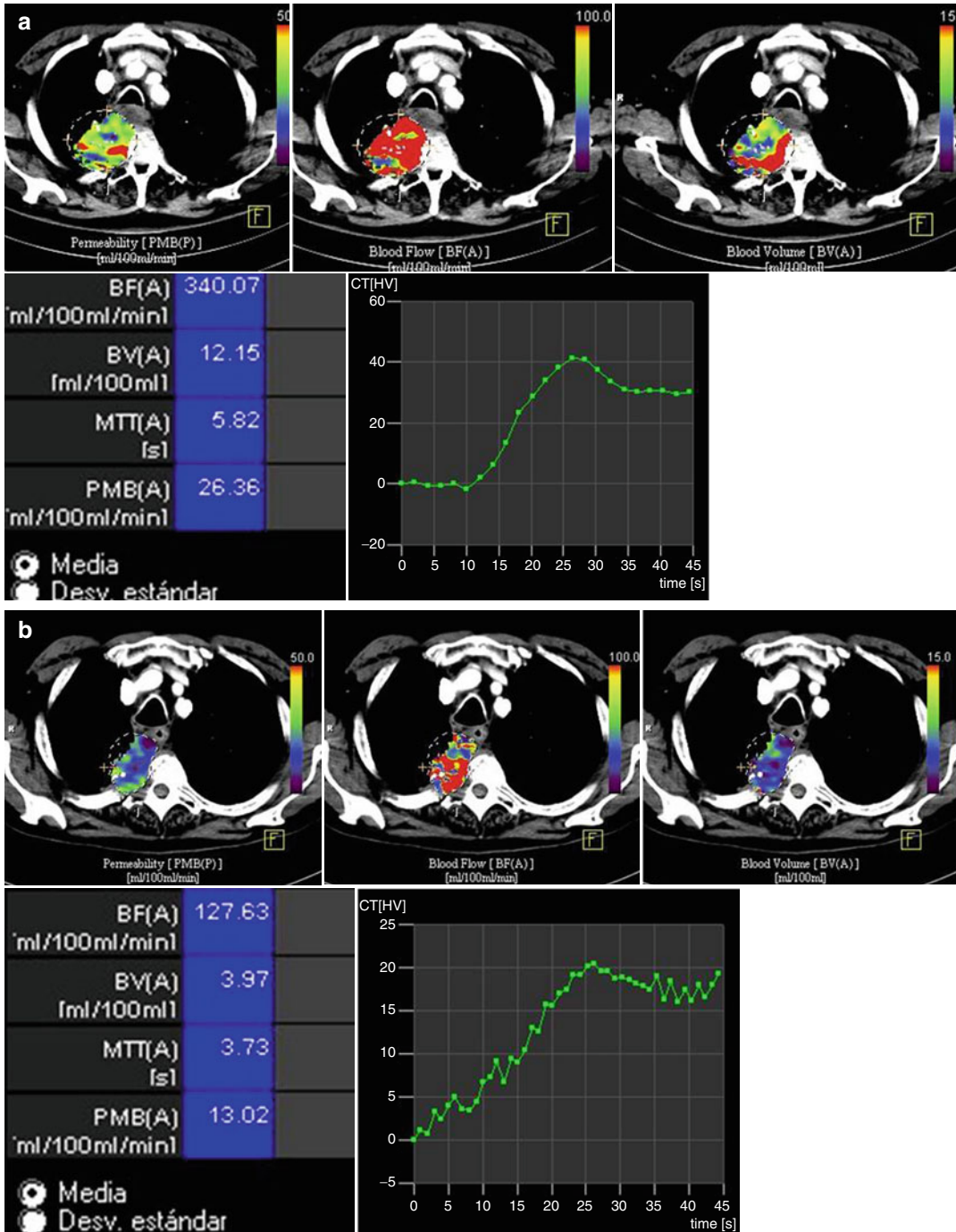


Fig. 29.20 Stage IIIb squamous cell carcinoma. Time-density curve, parametric color maps and numerical measures for perfusion parameters before treatment (a) and

after conventional QT and RT (b). There was a significant reduction in all perfusion parameters as well as on the time-density curve after treatment

29.7.2.4 Drug Development

VPCT may be a useful technique in improving an understanding of the biological effect and

mechanism of action of targeted therapies in vivo. Ng et al. have noted that an increase in PMB after treatment with RT is associated

with a higher efficacy of the treatment with combretastatin A4 phosphate in patients with lung cancer [109].

Conclusions

In summary, functional imaging has a growing role in the assessment of lung cancer. There is more experience with the use of FDG-PET for the evaluation of tumor metabolism, which may have an important role in the assessment of prognosis and therapeutic response. However, the lack of standardization of scanning methods and SUV measurements as well as lack of agreement on the optimal cutoff levels for determination of response limited its widespread applicability. Furthermore, the limited role of FDG-PET in tumor assessment of tumor response is due to standard protocols validated in large multicenter trials. In addition, DWI, DCE-MRI, and VPCT have been proposed recently for tumor characterization, staging, and therapy monitoring with promising results, although difficult technical acquisitions and short validation limit its clinical use at this moment.

References

1. Pretreatment evaluation of non-small-cell lung cancer. The American Thoracic Society and The European Respiratory Society. *Am J Respir Crit Care Med.* 1997;156:320–32.
2. Gupta NC, et al. Probability of malignancy in solitary pulmonary nodules using fluorine-18-FDG and PET. *J Nucl Med.* 1996;37:943–8.
3. Knight SB, et al. Evaluation of pulmonary lesions with FDG-PET. *Chest.* 1996;109:982–8.
4. Hubner KF, et al. Differentiating benign from malignant lung lesions using “quantitative” parameters of FDG PET images. *Clin Nucl Med.* 1996;21:941–9.
5. Lowe VJ, et al. Prospective investigation of PET in lung nodules (PIOPILN). *J Clin Oncol.* 1998;16:1075–84.
6. Gould MK, et al. Accuracy of positron emission tomography for diagnosis of pulmonary nodules and mass lesions: a meta-analysis. *JAMA.* 2001;285:914–24.
7. Nomori H, et al. Evaluation of F-18 fluorodeoxyglucose (FDG) PET scanning for pulmonary nodules less than 3 cm in diameter, with special reference to the CT images. *Lung Cancer.* 2004;45:19–27.
8. Erasmus JJ, et al. Evaluation of primary pulmonary carcinoid tumors using FDG PET. *Am J Roentgenol.* 1998;170:1369–73.
9. Higashi K, et al. Fluorine-18-FDG PET imaging is negative in bronchioloalveolar lung carcinoma. *J Nucl Med.* 1998;39:1016–20.
10. Godoy MC, Naidich DP. Subsolid pulmonary nodules and the spectrum of peripheral adenocarcinomas of the lung: recommended interim guidelines for assessment and management. *Radiology.* 2009;253:606–22.
11. Mountain CF. Revisions in the international system for staging lung cancer. *Chest.* 1997;111:1710–7.
12. Verboom P, et al. Cost-effectiveness of FDG-PET in staging non-small cell lung cancer: the PLUS study. *Eur J Nucl Med Mol Imaging.* 2003;30:1444–9.
13. Lardinois D, et al. Staging of non-small-cell lung cancer with integrated positron-emission tomography and computed tomography. *N Engl J Med.* 2003;348:2500–7.
14. Verhagen AF, et al. FDG-PET in staging lung cancer: how does it change the algorithm? *Lung Cancer.* 2004;44:175–81.
15. Reed CE, et al. Results of the American College of Surgeons Oncology Group Z0050 trial: the utility of positron emission tomography in staging potentially operable non-small cell lung cancer. *J Thorac Cardiovasc Surg.* 2003;126:1943–51.
16. Vansteenkiste JF, et al. Lymph node staging in non-small-cell lung cancer with FDG-PET scan: a prospective study on 690 lymph node stations from 68 patients. *J Clin Oncol.* 1998;16:2142–9.
17. Pieterman RM, et al. Preoperative staging of non-small-cell lung cancer with positron-emission tomography. *N Engl J Med.* 2000;343:254–61.
18. Mountain CF, Dresler CM. Regional lymph node classification for lung cancer staging. *Chest.* 1997;111:1718–23.
19. Prenzel KL, et al. Lymph node size and metastatic infiltration in non-small cell lung cancer. *Chest.* 2003;123:463–7.
20. De Leyn P, et al. Role of cervical mediastinoscopy in staging of non-small cell lung cancer without enlarged mediastinal lymph nodes on CT scan. *Eur J Cardiothorac Surg.* 1997;12:706–12.
21. Choi YS, et al. Mediastinoscopy in patients with clinical stage I non-small cell lung cancer. *Ann Thorac Surg.* 2003;75:364–6.
22. Birim O, et al. Meta-analysis of positron emission tomographic and computed tomographic imaging in detecting mediastinal lymph node metastases in nonsmall cell lung cancer. *Ann Thorac Surg.* 2005;79:375–82.
23. Gould MK, et al. Test performance of positron emission tomography and computed tomography for mediastinal staging in patients with non-small-cell lung cancer: a meta-analysis. *Ann Intern Med.* 2003;139:879–92.
24. Pfister DG, et al. American Society of Clinical Oncology treatment of unresectable non-small-cell

- lung cancer guideline: update 2003. *J Clin Oncol*. 2004;22:330–53.
25. de Langen AJ, et al. The size of mediastinal lymph nodes and its relation with metastatic involvement: a meta-analysis. *Eur J Cardiothorac Surg*. 2006;29:26–9.
 26. Dietlein M, et al. Cost-effectiveness of FDG-PET for the management of potentially operable non-small cell lung cancer: priority for a PET-based strategy after nodal-negative CT results. *Eur J Nucl Med*. 2000;27:1598–609.
 27. Scott WJ, et al. Cost-effectiveness of FDG-PET for staging non-small cell lung cancer: a decision analysis. *Ann Thorac Surg*. 1998;66:1876–85.
 28. Quint LE, et al. Distribution of distant metastases from newly diagnosed non-small cell lung cancer. *Ann Thorac Surg*. 1996;62:246–50.
 29. van Tinteren H, et al. Effectiveness of positron emission tomography in the preoperative assessment of patients with suspected non-small-cell lung cancer: the PLUS multicentre randomised trial. *Lancet*. 2002;359:1388–93.
 30. MacManus MP, et al. High rate of detection of unsuspected distant metastases by PET in apparent stage III non-small-cell lung cancer: implications for radical radiation therapy. *Int J Radiat Oncol Biol Phys*. 2001;50:287–93.
 31. Sekine I, et al. Progressive disease rate as a surrogate endpoint of phase II trials for non-small-cell lung cancer. *Ann Oncol*. 1999;10:731–3.
 32. Duhaylongsod FG, et al. Lung tumor growth correlates with glucose metabolism measured by fluoride-18 fluorodeoxyglucose positron emission tomography. *Ann Thorac Surg*. 1995;60:1348–52.
 33. Young H, et al. Measurement of clinical and subclinical tumour response using [18F]-fluorodeoxyglucose and positron emission tomography: review and 1999 EORTC recommendations. European Organization for Research and Treatment of Cancer (EORTC) PET Study Group. *Eur J Cancer*. 1999;35:1773–82.
 34. Higashi K, et al. Does FDG uptake measure proliferative activity of human cancer cells? In vitro comparison with DNA flow cytometry and tritiated thymidine uptake. *J Nucl Med*. 1993;34:414–9.
 35. Watanabe K, et al. [F-18]Fluorodeoxyglucose positron emission tomography can predict pathological tumor stage and proliferative activity determined by Ki-67 in clinical stage IA lung adenocarcinomas. *Jpn J Clin Oncol*. 2006;36:403–9.
 36. Ahuja V, et al. The prognostic significance of fluorodeoxyglucose positron emission tomography imaging for patients with nonsmall cell lung carcinoma. *Cancer*. 1998;83:918–24.
 37. Vansteenkiste JF, et al. Prognostic importance of the standardized uptake value on (18)F-fluoro-2-deoxy-glucose-positron emission tomography scan in non-small-cell lung cancer. An analysis of 125 cases. Leuven Lung Cancer Group. *J Clin Oncol*. 1999;17:3201–6.
 38. Dhital K, et al. [(18)F]Fluorodeoxyglucose positron emission tomography and its prognostic value in lung cancer. *Eur J Cardiothorac Surg*. 2000;18:425–8.
 39. Jeong HJ, et al. Determination of the prognostic value of [(18)F]fluorodeoxyglucose uptake by using positron emission tomography in patients with non-small cell lung cancer. *Nucl Med Commun*. 2002;23:865–70.
 40. Higashi K, et al. 18F-FDG uptake as a biologic prognostic factor for recurrence in patients with surgically resected non-small cell lung cancer. *J Nucl Med*. 2002;43:39–45.
 41. Ohtsuka T, et al. Prognostic significance of [(18)F]fluorodeoxyglucose uptake on positron emission tomography in patients with pathologic stage I lung adenocarcinoma. *Cancer*. 2006;107:2468–73.
 42. Ichiya Y, et al. A clinical evaluation of FDG-PET to assess the response in radiation therapy for bronchogenic carcinoma. *Ann Nucl Med*. 1996;10:193–200.
 43. MacManus MP, et al. Positron emission tomography is superior to computed tomography scanning for response-assessment after radical radiotherapy or chemoradiotherapy in patients with non-small-cell lung cancer. *J Clin Oncol*. 2003;21:1285–92.
 44. Patz Jr EF, et al. Prognostic value of thoracic FDG PET imaging after treatment for non-small cell lung cancer. *AJR Am J Roentgenol*. 2000;174:769–74.
 45. Vansteenkiste JF, et al. Potential use of FDG-PET scan after induction chemotherapy in surgically staged IIIa-N2 non-small-cell lung cancer: a prospective pilot study. The Leuven Lung Cancer Group. *Ann Oncol*. 1998;9:1193–8.
 46. De Leyn P, et al. Prospective comparative study of integrated positron emission tomography-computed tomography scan compared with mediastinoscopy in the assessment of residual mediastinal lymph node disease after induction chemotherapy for mediastinoscopy-proven stage IIIA-N2 Non-small-cell lung cancer: a Leuven Lung Cancer Group Study. *J Clin Oncol*. 2006;24:3333–9.
 47. Eschmann SM, et al. Repeat 18F-FDG PET for monitoring neoadjuvant chemotherapy in patients with stage III non-small cell lung cancer. *Lung Cancer*. 2007;55:165–71.
 48. Cerfolio RJ, et al. Restaging patients with N2 (stage IIIa) non-small cell lung cancer after neoadjuvant chemoradiotherapy: a prospective study. *J Thorac Cardiovasc Surg*. 2006;131:1229–35.
 49. Pottgen C, et al. Value of 18F-fluoro-2-deoxy-D-glucose-positron emission tomography/computed tomography in non-small-cell lung cancer for prediction of pathologic response and times to relapse after neoadjuvant chemoradiotherapy. *Clin Cancer Res*. 2006;12:97–106.
 50. Weber WA, et al. Positron emission tomography in non-small-cell lung cancer: prediction of response to

- chemotherapy by quantitative assessment of glucose use. *J Clin Oncol.* 2003;21:2651–7.
51. Hoekstra CJ, et al. Prognostic relevance of response evaluation using [18F]-2-fluoro-2-deoxy-D-glucose positron emission tomography in patients with locally advanced non-small-cell lung cancer. *J Clin Oncol.* 2005;23:8362–70.
 52. Shankar LK, et al. Consensus recommendations for the use of 18F-FDG PET as an indicator of therapeutic response in patients in National Cancer Institute Trials. *J Nucl Med.* 2006;47:1059–66.
 53. Wahl RL, et al. From RECIST to PERCIST: evolving considerations for PET response criteria in solid tumors. *J Nucl Med.* 2009;50:122S–50.
 54. Campione A, et al. Late outcome and perioperative complications for surgery of locally recurrent bronchogenic carcinoma. *J Cardiovasc Surg (Torino).* 2005;46:515–8.
 55. Watanabe Y, et al. Second surgical intervention for recurrent and second primary bronchogenic carcinomas. *Scand J Thorac Cardiovasc Surg.* 1992;26:73–8.
 56. Milton DT, Miller VA. Advances in cytotoxic chemotherapy for the treatment of metastatic or recurrent non-small cell lung cancer. *Semin Oncol.* 2005;32:299–314.
 57. Curran Jr WJ, et al. Should patients with post-resection locoregional recurrence of lung cancer receive aggressive therapy? *Int J Radiat Oncol Biol Phys.* 1992;24:25–30.
 58. Ryu JS, et al. FDG-PET in staging and restaging non-small cell lung cancer after neoadjuvant chemoradiotherapy: correlation with histopathology. *Lung Cancer.* 2002;35:179–87.
 59. Inoue T, et al. Detecting recurrent or residual lung cancer with FDG-PET. *J Nucl Med.* 1995;36:788–93.
 60. Hicks RJ, et al. The utility of (18)F-FDG PET for suspected recurrent non-small cell lung cancer after potentially curative therapy: impact on management and prognostic stratification. *J Nucl Med.* 2001;42:1605–13.
 61. Bury T, et al. Value of FDG-PET in detecting residual or recurrent nonsmall cell lung cancer. *Eur Respir J.* 1999;14:1376–80.
 62. Hellwig D, et al. Diagnostic performance and prognostic impact of FDG-PET in suspected recurrence of surgically treated non-small cell lung cancer. *Eur J Nucl Med Mol Imaging.* 2006;33:13–21.
 63. Kauczor HU, Ley S. Thoracic magnetic resonance imaging 1985 to 2010. *J Thorac Imaging.* 2010;25:34–8.
 64. Ohba Y, et al. Diffusion-weighted magnetic resonance for pulmonary nodules: 1.5 vs. 3 Tesla. *Asian Cardiovasc Thorac Ann.* 2011;19:108–14.
 65. Luna A, et al. Diffusion-weighted imaging of the chest. *Magn Reson Imaging Clin N Am.* 2011;19:69–94.
 66. Regier M, et al. Diffusion-weighted MR-imaging for the detection of pulmonary nodules at 1.5 Tesla: intraindividual comparison with multidetector computed tomography. *J Med Imaging Radiat Oncol.* 2011;55:266–74.
 67. Komori T, et al. 2-[Fluorine-18]-fluoro-2-deoxy-D-glucose positron emission tomography/computed tomography versus whole body diffusion-weighted MRI for detection of malignant lesions: initial experience. *Ann Nucl Med.* 2007;21:209–15.
 68. Takano A, et al. Detection of metastatic lesions from malignant pheochromocytoma and paraganglioma with diffusion-weighted magnetic resonance imaging: comparison with 18F-FDG positron emission tomography and 123I-MIBG scintigraphy. *Ann Nucl Med.* 2008;22:395–401.
 69. Ohno Y, et al. Dynamic MRI, dynamic multidetector-row computed tomography (MDCT), and coregistered 2-[fluorine-18]-fluoro-2-deoxy-D-glucose-positron emission tomography (FDG-PET)/CT: comparative study of capability for management of pulmonary nodules. *J Magn Reson Imaging.* 2008;27:1284–95.
 70. Chen W, et al. Whole-body diffusion weighted imaging vs. FDG-PET for the detection of non-small-cell lung cancer. how do they measure up? *Magn Reson Imaging.* 2010;28:613–20.
 71. Koyama H, et al. Comparison of STIR turbo SE imaging and diffusion-weighted imaging of the lung: capability for detection and subtype classification of pulmonary adenocarcinomas. *Eur Radiol.* 2010;20:790–800.
 72. Liu H, et al. Usefulness of diffusion weighted MR imaging in the evaluation of pulmonary lesions. *Eur Radiol.* 2010;20:807–15.
 73. Satoh S, et al. Can malignant and benign pulmonary nodules be differentiated with diffusion-weighted MRI? *AJR Am J Roentgenol.* 2008;191:464–70.
 74. Tondo F, et al. Role of diffusion-weighted imaging in the differential diagnosis of benign and malignant lesions of the chest-mediastinum. *Radiol Med.* 2011;116:720–33.
 75. Chen L, et al. Meta-analysis of diffusion-weighted MRI in the differential diagnosis of lung lesions. *J Magn Reson Imaging.* 2013;37(6):1351–8.
 76. Matoba M, et al. Lung carcinoma: diffusion-weighted MR imaging – preliminary evaluation with apparent diffusion coefficient. *Radiology.* 2007;243:570–7.
 77. Tanaka R, et al. Magnetic resonance imaging in peripheral lung adenocarcinoma: correlation with histopathologic features. *J Thorac Imaging.* 2009;24:4–9.
 78. Kanauchi N, et al. Role of diffusion-weighted magnetic resonance imaging for predicting of tumor invasiveness for clinical stage IA non-small cell lung cancer. *Eur J Cardiothorac Surg.* 2009;35:706–11.
 79. Abdel Razek A, et al. Characterization of mediastinal lymphadenopathy with diffusion-weighted imaging. *Magn Reson Imaging.* 2011;29:167–72.

80. Ohno Y, et al. Diffusion-weighted MRI versus 18F-FDG PET/CT: performance as predictors of tumor treatment response and patient survival in patients with non-small cell lung cancer receiving chemoradiotherapy. *Am J Roentgenol.* 2012;198:75–82.
81. Bains LJ, et al. Therapy response with diffusion MRI: an update. *Cancer Imaging.* 2012;12 (A):146–53.
82. Chang YC, et al. Dynamic contrast enhanced MRI in advanced non-small-cell lung cancer patients treated with first-line bevacizumab, gemcitabine, and cisplatin. *J Magn Reson Imaging.* 2012;36:387–96.
83. Tsuchida T, et al. Imaging the early response to chemotherapy in advanced lung cancer with diffusion-weighted magnetic resonance imaging compared to fluorine-18 fluorodeoxyglucose positron emission tomography and computed tomography. *J Magn Reson Imaging.* 2013;38(1):80–8.
84. Dingemans AM, et al. First-line erlotinib and bevacizumab in patients with locally advanced and/or metastatic non-small-cell lung cancer: a phase II study including molecular imaging. *Ann Oncol.* 2011;22:559–66.
85. Yabuuchi H, et al. Non-small cell lung cancer: detection of early response to chemotherapy by using contrast-enhanced dynamic and diffusion-weighted MR imaging. *Radiology.* 2011;261:598–604.
86. Okuma T, et al. Assessment of early treatment response after CT-guided radiofrequency ablation of unresectable lung tumours by diffusion-weighted MRI: a pilot study. *Br J Radiol.* 2009;82:989–94.
87. Li Y, et al. Peripheral lung carcinoma: correlation of angiogenesis and first-pass perfusion parameters of 64-detector row CT. *Lung Cancer.* 2008;61:44–53.
88. Hasegawa I, et al. Mediastinal lymph nodes in patients with non-small cell lung cancer: preliminary experience with diffusion weighted MR imaging. *J Thorac Imaging.* 2008;23:157–61.
89. Nakayama J, et al. Metastases in mediastinal and hilar lymph nodes in patients with non-small cell lung cancer: quantitative assessment with diffusion-weighted magnetic resonance imaging and apparent diffusion coefficient. *J Comput Assist Tomogr.* 2010;34:1–8.
90. Nomori H, et al. Diffusion-weighted magnetic resonance imaging can be used in place of positron emission tomography for N staging of non-small cell lung cancer with fewer false-positive results. *J Thorac Cardiovasc Surg.* 2008;135:816–22.
91. Regier M, et al. Diffusion weighted MRI and 18F-FDG PET/CT in non-small cell lung cancer (NSCLC): does the apparent diffusion coefficient (ADC) correlate with tracer uptake (SUV)? *Eur J Radiol.* 2012;81:2913–8.
92. Lichy MP, et al. Tumor detection by diffusion weighted. MRI and ADC-mapping initial clinical experiences in comparison to PET-CT. *Invest Radiol.* 2007;42:605–13.
93. Ohno Y, et al. N stage disease in patients with non-small cell lung cancer: efficacy of quantitative and qualitative assessment with STIR turbo spin-echo imaging, diffusion-weighted MR imaging, and fluorodeoxyglucose PET/CT. *Radiology.* 2011;261:605–15.
94. Wu LM, et al. Preoperative mediastinal and hilar nodal staging with diffusion-weighted magnetic resonance imaging and fluorodeoxyglucose positron emission tomography/computed tomography in patients with non-small-cell lung cancer: which is better? *J Surg Res.* 2012;178:304–14.
95. Kim YN, et al. A proposal for combined MRI and PET/CT interpretation criteria for preoperative nodal staging in non-small-cell lung cancer. *Eur Radiol.* 2012;22:1537–46.
96. Takenaka D, et al. Detection of bone metastases in non-small cell lung cancer patients: comparison of whole-body diffusion-weighted imaging (DWI), whole-body MR imaging without and with DWI, whole-body FDGPET/CT, and bone scintigraphy. *J Magn Reson Imaging.* 2009;30:298–308.
97. Koyama H, et al. Magnetic resonance imaging for lung cancer. *J Thorac Imaging.* 2013;28:138–50.
98. Girvin F, Ko JP. Pulmonary nodules: detection, assessment, and CAD. *AJR Am J Roentgenol.* 2008;191:1057–69.
99. Ohno Y, et al. Prognostic value of dynamic MR imaging for non-small-cell lung cancer patients after chemoradiotherapy. *J Magn Reson Imaging.* 2005;21:775–83.
100. Kelly RJ, et al. Evaluation of KRAS mutations, angiogenic biomarkers, and DCE-MRI in patients with advanced non-small-cell lung cancer receiving sorafenib. *Clin Cancer Res.* 2011;17:1190–9.
101. Ng Q, et al. Lung cancer perfusion at multi-detector Row CT: reproducibility of whole tumor quantitative measurements. *Radiology.* 2006;239:547–53.
102. Ng C, et al. Reproducibility of perfusion parameters obtained from perfusion CT in lung tumors. *AJR Am J Roentgenol.* 2011;197:113–21.
103. Tacelli N, et al. Non-small cell lung cancer perfusion: pathologic-CT correlation in 15 patients. *Radiology.* 2010;257:863–71.
104. Mandeville HC, et al. Operable non-small cell lung cancer: correlation of volumetric helical dynamic contrast enhanced CT parameters with immunohistochemical markers of tumor hypoxia. *Radiology.* 2012;264:581–9.
105. Ohno Y, et al. Differentiation of malignant and benign pulmonary nodules with quantitative first-pass 320-detector Row perfusion CT versus FDG PET/CT. *Radiology.* 2011;258:599–609.
106. Wang J, et al. Tumor response in patients with advanced non-small cell lung cancer: perfusion CT evaluation of chemotherapy and radiation therapy. *AJR Am J Roentgenol.* 2009;193:1090–6.

107. Fraioli F, et al. Whole-tumor perfusion CT in patients with advanced lung adenocarcinoma treated with conventional and antiangiogenetic chemotherapy : initial experience. *Radiology*. 2011;259:574–82.
108. Tacelli N, et al. Perfusion CT allows prediction of therapy response in non-small cell lung cancer treated with conventional and anti-angiogenic chemotherapy. *Eur Radiol*. 2013;23:2127–36.
109. Ng QS, et al. Tumor antivascular effects of radiotherapy combined with combretastatin a4 phosphate in human non-small-cell lung cancer. *Int J Radiat Oncol Biol Phys*. 2007;67:1375–80.